PRESSURE DEPENDENCE OF MAGNETIC TRANSITIONS

By

JAMES EDMUND MILTON

A DISSERTATION PRESENTED TO THE GRADUATE COUNCIL OF
THE UNIVERSITY OF FLORIDA
IN PARTIAL FULFILLMENT OF THE REQUIREMENTS FOR THE
DEGREE OF DOCTOR OF PHILOSOPHY

UNIVERSITY OF FLORIDA

April, 1966

ACKNOWLEDGMENTS

The author is deeply indebted to many people for aid and encouragement in completing this dissertation. He wishes to express his gratitude to the many people who have helped and especially to those listed below.

Dr. Thomas A. Scott, the chairman of the author's supervisory committee, suggested the problem and was always ready to give aid when needed.

Mr. Basil McDowell was absolutely indespensible, he assisted in the design and construction of much of the equipment used in this study. In addition to this he supplied liquid helium when needed and frequently gave a friendly helping hand or clever suggestions.

Dr. William S. Goree gave many helpful suggestions regarding the cryogenic apparatus and designed the pressure bomb used.

Mr. K. S. Krishnan served as a soundingboard for many ideas involving experimental techniques and frequently suggested improvements.

Mr. Guy Ritch and Mr. Frank Ebright were very able assistants during the final phase of data taking.

Dr. Stanley S. Ballard and Dr. Thomas A. Scott provided financial support during most of the author's

graduate career. Dr. Knox Millsaps graciously lightened the author's work load during the writing of this dissertation.

Deadlines would not have been met had it not been for the encouragement and invaluable help given by Dr. Richard L. Fearn in the preparation of this dissertation.

Finally the author wishes to thank Mrs. Jacqueline Ward who very cheerfully and untiringly typed this manuscript. Mr. Guy Hardee lent an able hand in drawing the figures.

This work was financed by Grant No. NSF-GP1866 from the National Science Foundation.

TABLE OF CONTENTS

LIST OF FIGURES

LIST OF TABLES

CHAPTER I

INTRODUCTION

Historical background

Magnetism has aroused man's curiosity and fired his imagination for at least several thousand years. References to the attractive power of the lodestone had already appeared in Greek writing by 600 B.C.[1] The first known reference to the fact that magnetism could also repel a body is found in the writings of the Roman Lucretius Carus in the 1st Century B.C.[2] It is interesting that no references to the directive property of the magnet, as used in the compass, is found in old Greek and Roman literature, but beginning in the period 1000-1200 A.D. the history of magnetism is closely associated with the compass and its use in navigation. The first clear mention of a magnet used to indicate direction was made by Shen-Kua (1030-1093), a Chinese mathematician and instrument maker. By 1100 A.D., the Chinese Chu Yu reports that the compass was in use by sailors going between Canton and Sumatra. In 1269, Peregrinus de Maricourt reported on experiments made on a spherical lodestone.[3] He explored the surface of the sphere with small particles of iron and applied the term pole to the places in which the magnetic power appeared to

be concentrated. Little progress is reported until 1600 when William Gilbert published his De Magnete which summarized the knowledge of magnetism and reported the results of many of his own experiments. In this book he propounds his own great contribution, the realization that the earth itself is a magnet. Also of great importance is his determination that if magnetized iron is heated to a bright red it loses its magnetism.

In 1785, Charles A. Coulomb[4] established with some precision the inverse square law of attraction or repulsion between unlike and like magnetic poles. This result was taken over by Poisson who became the best interpreter of the physical constructs which Coulomb had discovered.[5] To magnetism, Poisson brought the concept of the static potential, which had been so successful in solving the problems of static electricity. He also assumed magnetization to be a molecular phenomenon, but believed that the molecule became magnetic only when the two fluids it contained became separated. It was Weber[6] who proposed that each molecule is a permanent magnet, subject to a frictional force that tends to maintain it in its established orientation. This theory failed to explain the existance of residual induction and hystersis.

In 1820, Oersted discovered that an electric current would affect a magnetic needle. Ampère then investigated experimentally and mathematically the forces between currents. He was able to show that a current in a

circuit was equivalent to a magnetic shell of calculable strength. He then put forth the hypothesis that magnetism arose from currents within the molecules. This theory stood until it was modified by modern quantum mechanics.

Pierre Curie made the first extensive study of the thermal properties of magnetic materials.[7] As a result of these studies he was able to establish that the magnetic susceptibility of a paramagnetic material was inversely proportional to the absolute temperature.

$$\chi = C/T \tag{1.1}$$

The constant of proportionality was determined for each material and was always found to be positive. He found a relatively rapid decrease in the magnetization as each ferromagnetic material was heated to a critical temperature, now called the Curie temperature. Above this temperature, which was different for each material, the behavior was much like an ordinary paramagnetic substance.

The first important modern development in magnetic theory came when Langevin[8] used statistical mechanics to derive the Curie law, equation (1.1). The underlying assumptions of his theory were that each molecule had a definite magnetic moment that tended to be aligned by the applied magnetic field and at the same time disturbed by thermal agitation. Many years later this derivation was modified by Brillouin who took into account the quantum mechanical requirement that the atomic magnetic moments were

restricted to a finite set of orientations relative to the applied field.[9]

After the work by Langevin, Weiss[10] made the next big step in developing a modern theory of magnetism. He assumed that the molecules are exposed both to the applied field and to a so-called molecular field proportional to the magnetization. It is a consequence of the Weiss theory that small regions, domains, within a magnetic material are magnetized to saturation even though the net magnetization of the body is zero. This is possible by having the magnetic moments of the domains oriented randomly. The Weiss theory is a very successful one which has been substantiated by many experiments. It is, however, not a very pleasing one since no explanation of the origin of the molecular field is given.

In 1925, Uhlenbeck and Goudsmit introduced the concept of electron spin to explain some discrepancies between theory and experimental measurements of the spectra of one-electron atoms and the alkali-metals. This spin has associated with it both an angular momentum and a magnetic moment. Following this came the enunciation of the Pauli exclusion principle. These two developments allowed Dirac and Heisenberg[11,12] to demonstrate a quantum mechanical origin for the Weiss molecular field. In their theory one starts with the Heitler-London model of the hydrogen molecule and considers a Hamiltonian made up wholly of electrostatic terms and kinetic energy terms. The Pauli exclusion

principle enters the discussion only through symmetry requirements. Further, one must make an assumption regarding a distribution of energy levels. Heisenberg assumed this distribution was Gaussian. Using these conditions, it was possible to reproduce the Weiss theory and show that the origin of the molecular field was a quantum mechanical exchange integral. Thus, the most successful theory propounded had been given a quantum-mechanical basis and indeed it seemed that magnetism might at last be understood. But, as is usually the case, things were not as good as they appeared. Heisenberg's theory suffered from several serious weaknesses. 1) It was based upon the hydrogen molecule and contained no account of lattice periodicity. 2) The results obtained were very much dependent upon the distribution of energy levels assumed. 3) The actual calculation of the exchange parameter was an extremely difficult problem and thus far has not been resolved.

At about the same time the Heisenberg-Dirac theory was being developed, Ising[13] proposed a different method for looking at the problem. The spins were disposed at regular intervals along the length of a one-dimensional chain. In accordance with the laws of Uhlenbeck and Goudsmit each spin was allowed to take on only one of two possible orientations. It was possible to obtain an exact solution for this model if it was assumed that each spin interacted with only a finite number of neighbors.

Unfortunately the result indicated that ferromagnetism should not occur above 0°K. Since that time exact two-dimensional solutions and approximate three-dimensional solutions have given finite transition temperatures, thus showing that the failure of the first model was due to its dimensionality.

Various methods have been employed to try to improve on the Heisenberg theory. One of the most successful of these is the method of spin waves developed by Bloch and Slater.[14,15] This theory starts with the observation that the eigenvalue of the Heisenberg exchange coupling can be determined rigorously if the spins of all but one atom are parallel. Furthermore, approximate solutions can be found if the number of reversed spins is small when compared with the number of atoms. Due to the above assumption this theory is good only for very low temperatures. It has been quite successful in describing the variation of magnetization with temperature in this region.

In 1932, Néel proposed a theory to account for a type of paramagnetic susceptibility temperature dependence which did not agree with any of the existing theories.[16] He proposed two interpenetrating sublattices undergoing negative exchange interaction. This theory continues to be the basis for modern developments in the theory of what is now called antiferromagnetism.

The rare earths, which have become available in quantity in pure form only since the development of the ion exchange method of separation, cannot be described completely by the theories discussed in the preceding section. They have spurred a renewal in interest in magnetism on both the experimental and theoretical fronts. Their physical properties will be discussed in detail in the following section and the theories developed to describe them will be examined in a later chapter.

Structure and information on rare earths

The rare earth metals are composed of the fifteen elements which range from lanthanum to lutetium. The electronic structure of these elements is normally given by

$$(4f)^n(5s)^2(5p)^6(5d)^1(6s)^2$$

where n increases from 0 to 14 as the atomic number increases from 57 to 71. The outer electronic structure, which essentially determines their chemical properties, is the same for all of these elements and they normally appear in compounds as tripositive ions. Often scandium and yttrium, atomic numbers 21 and 39 respectively, are grouped with the rare earths since their external electronic configuration is similar.[17,18]

The 4f electrons are tightly bound inside the outer closed shells on the atoms and therefore play only a small role in chemical bonding. They behave almost as they

would in a free ion, giving a resultant angular momentum due to both spin and orbital motion. Since there is a magnetic moment associated with this angular momentum, all rare earth compounds have interesting magnetic properties.

It will be shown in Chapter II that a model based on ions with $4f^n$ configurations acted on by crystalline fields and coupled by exchange interactions is capable of explaining much of the magnetic phenomena of the rare earth metals.

Rare earths have been investigated extensively within the last ten years at the Ames Research Laboratory and the Oak Ridge National Laboratory. The former of these has been involved in the separation and purification of these elements, and with the measurement of specific heat, thermal expansion, electrical resistivity, magnetic properties, and other physical properties. The latter group has performed neutron diffraction studies and determined the complicated magnetic structures.

The tripositive ion picture, outlined above, is violated by two of the rare earths, Eu and Yb, which come immediately before the middle element and the last element of the series, respectively. These elements should have $4f^6$ and $4f^{13}$ configurations, however, they appear to prefer to gain the extra correlation energy of a half-filled or completed shell and take a divalent form with $4f^7$ and $4f^{14}$ configuration. Ytterbium has only a small paramagnetism as would be expected from a closed shell and

europium shows large magnetic moments as it should for the $4f^7$ structure. One other element that should be mentioned in this respect is Ce, which may be found in a four-valent state either at low temperature or at high pressure. This is due to the fact that at the beginning of the series the 4f and 5d electrons have similar energies. In this state, as would be expected, Ce is found to exhibit small paramagnetism. Above 100°K the stable form is found to be $4f^1$ and trivalent.

The room temperature crystal structure of the rare earths tend to fall into two categories, the hexagonal close packed and a double hexagonal structure as shown in Figure 1. While they have been reported with various crystal structures, it seems that La, Ce, Pr and Nd, the light rare earths, usually have the modified hexagonal structure. Promethium has no stable isotope and therefore no information is available. Next, Sm has a very complicated hexagonal structure which repeats after nine hexagonal layers. The remainder, Gd, Tb, Dy, Ho, Er, Tm and Lu, have hexagonal close packed structures with c/a ratios 1.57-1.59. Their magnetic properties, while complex, show a certain regularity which may be traced to exchange interactions and crystalline fields.

In the absence of detailed knowledge of the band structure of any of these elements theoretical work has been based upon the crude approximation of nearly free electrons. The effect of lattice symmetry has to some

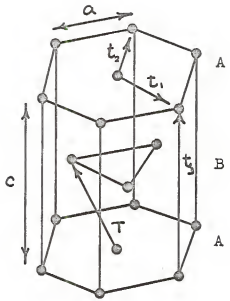

Hexagonal close packed structure

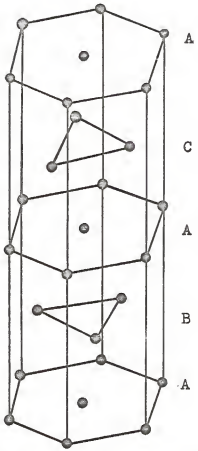

Double hexagonal structure

Figure 1. Rare earth crystal structures.

extent been included by considering the Brillouin zone structure[19] for the heavy rare earth series. The primitive translations $\hat{t}_1$, $\hat{t}_2$ and $\hat{t}_3$ are shown in Figure 1. There are two atoms per unit cell, one at the origin and one at $\tau = \frac{1}{3}(\hat{t}_1 + 2\hat{t}_2) + \frac{1}{2}\hat{t}_3$. The reciprocal lattice is also hexagonal and has vectors $\vec{\tau}_1$ and $\vec{\tau}_2$ with magnitude $\frac{4\pi}{a\sqrt{3}}$ in the basal plane 120° apart, and $\vec{\tau}_3$ perpendicular to this plane with magnitude $2\pi/c$.

Even when the atoms are triply ionized the tightly bound 4f electrons are shielded from the crystalline field by the $5s^2$ and $5p^6$ electrons. Under these conditions their orbital angular momentum remains unquenched by the fields of neighboring ions. These electrons have total orbital angular momentum, L, and total spin, S, in the ground state as prescribed by Russel-Saunders coupling and Hund's rules. The energy difference between the ground state J multiplet and the first excited J multiplet is usually greater than 0.1 ev, therefore the excited multiplet plays no role in thermal properties.

There are basically four types of measurements that have been made in order to determine the magnetic properties of these elements. They are neutron diffraction, bulk magnetic measurements, specific heat measurements, and electrical resistivity measurements. A brief discussion of the information that can be obtained by each of these methods is given below.

Detailed neutron diffraction studies have been carried out on several of the rare earths.[20,21,22,23,24,25,26] The magnetic structures thus determined have been found to be quite complex. These studies have also given information about the magnitude of the ordered moment and its temperature dependence. The magnetic properties are found to be highly anisotropic, that is, the moments along the c-axis are quite different from the moments in the basal plane. Figure 2 shows some of the types of ordering that have been found and Table 1 gives the transition temperatures and structures for each element.

Bulk magnetic measurements have shown that the susceptibility of these elements at high temperatures is roughly described by the Curie-Weiss law.

$$\chi = \frac{N\beta^2\lambda^2 J(J+1)}{3k(T-\theta)}$$

Here the Weiss constant, θ, indicates the approximate value of the exchange energy. It is also possible to obtain the magnitude of the ordered moments from this type of experiment. If a sufficiently strong magnetic field is applied to one of the antiferromagnetic structures it is possible, in some cases, to change it to a ferromagnetic structure. The field at which this occurs is called the critical field and can be used to obtain information about the energy difference between the two states.

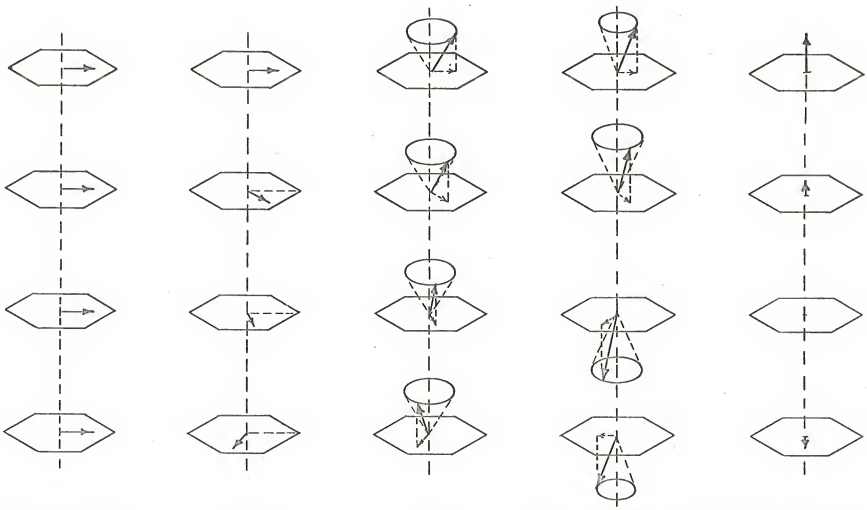

Figure 2. Magnetic structures of rare earths.

Table 1

Summary of available experimental information on rare earth magnetic structures.

Element	Highest ordering temperature	Order	Lower ordering temperature	Order
Ce	12.5	Complex	--	--
Nd	7	Complex	19	Complex
Sm	15	--	--	--
Gd	293	Ferro	--	--
Tb	228	Helix	220	Ferro
Dy	179	Helix	85	Ferro
Ho	132	Helix	20	Cone
Er	85	LW	50	Complex
			20	Cone
Tm	56	LW	22	--

This information was obtained from a review article by Belov[52] and Elliott.[19]

The transitions from one magnetic state to another are accompanied by sharp peaks in the specific heat versus temperature curves. These peaks can be located very accurately and therefore allow accurate determination of transition temperatures.

The electrical resistance of these elements show anomalies at the magnetic transitions. These anomalies have been used to locate the transitions by a number of investigators.

Experimental work

The way in which magnetic properties of materials vary with pressure has long been of interest to physicists. Some of the earliest experiments in this area were done in an attempt to gain information about the origin of the earth's magnetic field.[27] The more recent ones, however, have been done in order to try to obtain information on the volume dependence of the exchange integral. One of the methods of attack on this problem has been to measure the shift with pressure of the temperature at which the material goes from one magnetic state to another. The temperature of the transition to the ferromagnetic state is called the Curie temperature, T_c, while the temperature of transition from the paramagnetic to the antiferromagnetic state is called the Néel temperature, T_N. The discussion which follows will be confined to experiments in which dT/dP have been determined. There is a vast literature of other

types of magnetic experiments including a recent review by Kouvel.[28]

One of the earliest attempts in this field was that of Yeh in 1925.[29] He measured the effect of pressure on the magnetic permeability of iron, nickel and cobalt. This work was followed by that of Steinberger who, in 1933, did essentially the same experiment with improved sample annealing techniques.[30] These experiments did not specifically set out to measure the shift of the magnetic transition temperature with pressure. In retrospect, however, it can be recognized that Steinberger actually induced a phase change from the ferromagnetic state to the paramagnetic state in a 30Ni 70Fe sample by the application of pressure at room temperature. From his data it can be concluded that $dT_c/dP < 0$ for this alloy.

The first actual attempt to measure dT_c/dP was made in 1931 by Adams and Green[27] who studied iron, nickel, magnetite, nickel steel and meteoric iron. They used the transformer method for detecting the transition. A primary and a secondary coil were wound on a closed frame made of the sample material. An alternating voltage was applied to the primary and the output voltage was monitored as a function of temperature. The drop in output at T_c is very sharp, and although it does not define the Curie temperature in the conventional way, the method is satisfactory for finding a change in Curie point. They

used carbon dioxide as the pressure transmitting medium and therefore achieved truly hydrostatic pressure. The shift for pressures up to 3.5 kilobars was found to equal zero for all of their samples. This result has not been confirmed by other investigators and it is believed that thermal uncertainties masked the true changes.

Michels et al.[31] used the discontinuity in the $(1/R)(dR/dT)$ versus temperature curve to indicate T_c. The sample material, which was 70Ni 30Cu, exhibited a broad transition that occurred gradually over 50°C. They concluded from this that it was necessary to determine a shift of the Curie region. By carefully analyzing their data they were able to obtain $dT_c/dP = +6.4 \times 10^{-2}$ °K/kilobar. This method requires very accurate resistance measurements over large temperature intervals and is complicated by the fact that resistance also changes with pressure. Later a monel alloy was studied by the same method.[32] This transition also was quite broad and yielded $dT_c/dP = 3 \times 10^{-2}$ °K/kilobar.

Ebert and Kussman[33] used large magnetic fields to obtain magnetization versus temperature curves so that the T_c could be determined in the conventional manner. They then applied pressure and tried to determine dT_c/dP for several pure metals and alloys. The result obtained for all samples was $dT_c/dP = 0$. Michels and De Groot[34] criticized their result and showed by a thermodynamic treatment of second order phase transitions that in general

$dT_c/dP \neq 0$. They further showed that the experimental method used by Ebert and Kussman was not accurate enough to show small but significant variations of T_c. Kornetzki[35] took the data obtained by Ebert and Kussman and re-analyzed them and obtained non-zero values for dT_c/dP .

In 1954, Patrick[36] made a detailed study to determine dT_c/dP of nickel, gadolinium, cobalt, iron, eight metallic alloys, a ferrite and a perovskite. The transitions were detected by the transformer method as developed by Adams and Green. Two pressure systems were used, one used a gas for the pressure transmitting medium and the other used a liquid. The pressure was truly hydrostatic. Patrick's results agreed with those of Michels et al., and are widely quoted in the literature.

Samara and Giardini[37] made measurements on the shift of T_c in nickel and a nickel iron alloy. A multianvil pressure system with pyrophyllite as the transmitting medium was used. Pressures up to 35 kilobars were generated and the shifts found were in general agreement with those already determined. The transition was detected by monitoring the self-inductance of a coil which was wound on the sample.

In addition to the electrical resistivity, self-inductance and transformer methods of detecting magnetic transitions, there are two other techniques which have been used. These transitions can be located by monitoring the

mutual inductance between two coils wound on the sample. Changes in the magnetic moment of the sample show as a change in this mutual inductance, which can be measured very accurately by bridge methods. Finally, when the pressure system permits, a method involving the extraction of the sample from a magnetic field can be used.

The pressure systems for this type of study fall into two distinct categories, those whose pressure transmitting medium is a liquid or a gas and those that use a solid for pressure transmission. The former, of course, are the only ones which produce truly hydrostatic pressures, however, the latter are able to obtain much higher pressures. One study has been made by sealing water in the pressure vessel and then freezing the entrapped water. The disadvantage of this method is the possibility of having tremendous pressure gradients inside the pressure vessel.

The results of all of the investigations of pressure shifts of the transition temperatures for pure rare earths as well as the pertinent information about methods used are summarized in Table 2.

This dissertation deals with the effect of pressure on the Curie transition and the Neel transition in dyprosium and erbium. These experiments are the second in a planned series of high pressure studies to be carried out at the University of Florida. It was necessary to develop the complete pressure system as well as the methods

Table 2

Summary of experimental results on the pressure shifts of the magnetic transitions for the rare earths.

Element	Pressure range kilobars	Pressure medium	Detection method	°K/kilobar	°K/kilobar	Reference
Gadolinium	0-8	Gas	Transformer	-1.18		36
	0-6	Gas	Mut. Induct.	-1.56		38
	0-33	AgCl	Transformer	-1.60		39
	5-52	AgCl	Transformer	-1.72		40
Terbium	0-4	Gas	Mut. Induct.		-.82	38
	0-25	AgCl	Transformer	-1.0		43
	0-71	AgCl	Transformer	-1.07		40
Dysprosium	0-8.4	Indium	Mut. Induct.		-.54	41
	15-45	Solid	Resistance		-.60	42
	0-4	Gas	Mut. Induct.		-.60	38
	0-25	AgCl	Transformer		-.40	43
	5-77	AgCl	Transformer		-.66	40
	0-7	AgCl	Transformer	+1.4		43
	7-25	AgCl	Transformer	-.8		43
	0-1.8	Ice Bomb	Extraction	-3.9		44
Holmium	0-6	Gas	Mut. Induct.		-.45	38
	5-82	AgCl	Transformer	-.48		40

and equipment necessary for performing the experiments. A large high-pressure helium gas system, which is described in detail in Chapter III, was constructed. A gas system was chosen in order to be able to work under truly hydrostatic pressure at low temperatures. The choice of samples was based upon the availability of high purity specimens and also the desire to take advantage of the ability of the pressure system to work at very low temperatures. When this work was started there were no published results on pressure shifts in any of the rare earths. As can be seen in the preceding section there has recently been a flurry of activity in this field. The pressure system constructed here is still the only one capable of studying the lower temperature transitions under hydrostatic conditions and further studies on holmium and thulium are underway presently.

The results obtained for erbium for both dT_N/dP and dT_c/dP are new. The results obtained for dT_N/dP for dysprosium are presented as corroborating those which have now been published. The dT_c/dP for dysprosium is in marked disagreement with that presented by Robinson et al.[43] which is the only one published to date. A complete discussion of the results is given in Chapter IV.

CHAPTER II

THEORY

Introduction

Any discussion on magnetism must be based on quantum mechanical concepts. In the general discussion of magnetism which follows the author has relied heavily on numerous references.[45-53] The discussion of rare earths mainly follows the reviews by Elliott,[54] Yosida[55] and the books by Van Vleck[56] and Chikazumi.[57]

This discussion can in no way be thought of as complete, but rather will attempt to describe the methods that have been most successful in treating the problem of magnetism. While much progress has been made there exists, at present, no completely satisfactory theory.

Types of magnetism

This section begins with a brief summary of the types of magnetism that are observed and some remarks concerning their origin. The major classifications are diamagnetism, paramagnetism, ferromagnetism, antiferromagnetism and ferrimagnetism.

Diamagnetism is a weak magnetism in which a magnetization is exhibited opposite to the direction of

the applied field. It is associated with the tendency of electric charges to shield the interior of a body from an applied magnetic field. It can be looked upon as a manifestation of the well-known Lenz's law, which states that when the flux through an electrical circuit is changed an induced current is set up in such a direction as to oppose this flux change. In a resistanceless circuit such as the orbit in an atom or in a superconductor the induced current persists as long as the field is present. Landau[58] has shown that there can also be a diamagnetic contribution from the conduction electrons in a metal. Diamagnetism is present in all substances; however, in all cases except the superconductor it is a small effect with a susceptibility on the order of -10^{-5} $cm^3/mole$. This effect is swamped if any other type of electron magnetism is present. The superconductors, which exclude all magnetic fields, exhibit perfect diamagnetism and have a susceptibility equal to $-1/4\pi$. Diamagnetism plays a small role in the rare earths and will not be mentioned in the remainder of this discussion.

Paramagnetism arises in materials in which there are permanent magnetic moments present. Magnetization results from the orientation of these moments in an applied field. This orientation is opposed by thermal agitation and therefore would be expected to be highly temperature dependent. The permanent moments may arise from the spin and orbital motion of the electrons or from

the nuclei. In the rare earths the nuclear susceptibility is about 10^{-6} times the electron susceptibility and will not be considered in this discussion. The electron paramagnetic susceptibilities vary from about $+10^{-5}$ to $+10^{-2}$ cm^3/mole. The rare earths are accurately described in the paramagnetic region by the Curie-Weiss law which will be developed in a following section.

A substance is called ferromagnetic if it possesses a spontaneous magnetic moment even in the absence of an applied magnetic field. This moment occurs only below some critical temperature known as the Curie temperature. This type of behavior is explained by adding to the paramagnetic model a strong co-operative effect which tends to align the permanent moments in a parallel manner. Since dysprosium and erbium are both ferromagnetic at low temperatures the theories of this type of magnetism will be discussed in a following section.

Antiferromagnetism arises from co-operative effects in a manner similar to ferromagnetism. In this case, however, the spins tend to align themselves in an antiparallel manner. The net magnetization is small and gives susceptibilities on the order of the ones given by paramagnetism. The temperature dependence of this susceptibility is, however, very different from that of paramagnetism. More will be said about this phenomenon in following discussions.

The oldest magnetic material known, the lodestone, is a ferrimagnet. This type of magnetism is characterized by an antiparallel arrangement of moments but with the moments of unequal magnitude. This can give a strong external magnetic field. This type of effect is thought to arise from the same type of interaction as the antiferromagnetic case. These materials are of great practical importance since many of them are insulators. None of the rare earths exhibit this type of magnetism so no further mention of it will be made.

Quantum mechanical Langevin theory of paramagnetism

Consider a system of N independent atoms in a magnetic field $\vec{H}$. There will be $2J+1$ Zeeman levels for each J. Assume that, as with the rare earths at room temperature, kT is small compared to the energy gap between the ground state and the first excited state J'.

Write the operator equation $\vec{\mu} = g\mu_B \vec{J}$ where $\mu_B = e\hbar/(2mc)$ is the Bohr magneton and g is the Landé g factor given by

$$g = 1 + \frac{J(J+1) + S(S+1) - L(L+1)}{2J(J+1)}$$

The energy of interaction between the magnetic moments and the applied field is given by $W(H) = -\vec{\mu}\cdot\vec{H} = -g\mu_B M_J H$. Using statistical mechanics it can be shown that the magnetic susceptibility is given by $\chi = \frac{kT}{H}\frac{\partial(\ln Z)}{\partial H}$, where $Z = \sum_i e^{-\frac{E_i}{kT}}$ is the partition function for the system.

In this system

$$Z = \left[\sum_{M_J=-J}^{+J} \exp\left\{\frac{g\mu_B M_J H}{kT}\right\}\right]^N$$

which gives

$$\chi = \frac{NkT}{H} \frac{\sum_{-J}^{+J} \frac{g\mu_B M_J}{kT} \exp\left\{\frac{g\mu_B M_J H}{kT}\right\}}{\sum_{-J}^{+J} \exp\left\{\frac{g\mu_B M_J H}{kT}\right\}}$$

After some mathematical manipulation one obtains

$$\chi = \frac{Ng\mu_B J}{H} B_{J(X)} \qquad (2.1)$$

for the magnetic susceptibility, where $B_{J(X)}$ is called the Brillouin function and can be written

$$B_{J(X)} = \frac{2J+1}{2J} \coth\left(\frac{2J+1}{2J}\right)X - \frac{1}{2J} \coth\left(\frac{X}{2J}\right)$$

where

$$X = \frac{g\mu_B JH}{kT} \quad . \qquad (2.2)$$

If the energy of Zeeman splitting is small compared to kT then $X \ll 1$ and one obtains a nearly equal probability of occupation for all levels. Under these conditions $B_{J(X)}$ can be expanded in a power series and higher order terms neglected to obtain

$$B_{J(X)} \approx \frac{J+1}{3J} X \quad . \qquad (2.3)$$

By using equations 2.1, 2.2 and 2.3 one can obtain

$$\chi = \frac{NJ(J+1)g^2\mu_B^2}{3kT} \tag{2.4}$$

It can be seen that equation 2.4 is equivalent to equation 1.1, the Curie law, where $C = NJ(J+1)g^2\mu_B^2/3k$.

By using equation 2.1 and the relationship $M = \chi H$ a general expression for the magnetization of a material obeying the above theory can be written as

$$M = Ng\mu_B J B_J(x) \tag{2.5}$$

In the special case where $x << 1$ equation 2.1 and 2.4 can be combined to obtain

$$M = \frac{Ng^2\mu_B^2 J(J+1)H}{3kT} \tag{2.6}$$

Weiss theory of ferromagnetism

Weiss modified the above theory by adding to the paramagnetic model an interaction which tended to make the atomic moments align themselves in a parallel manner. He defined a molecular field proportional to the magnitization of the sample, $H_m = \gamma M$, where γ is the Weiss constant. Now, using the methods of the previous derivation, one can obtain some useful relationships. If the magnetic field in equation 2.2 is replaced by an effective

field, $H_{eff} = H + \gamma M$, then for ferromagnetic materials

$$X = \frac{g\mu_0 J}{kT}(H + \gamma M) \tag{2.7}$$

In order to look for the spontaneous magnetization let $\vec{H} = 0$ and solve equation 2.7 for M to obtain

$$M = \frac{XkT}{g\mu_0 J\gamma} \tag{2.8}$$

Since M must satisfy both equations 2.5 and 2.8 the simplest procedure is to investigate its behavior at various temperatures by graphical methods.

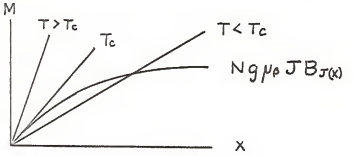

Figure 3. Spontaneous magnetization, Weiss theory.

From Figure 3 it can be seen that there is a critical temperature, T_c , below which one gets spontaneous magnetization due to the γM field. As the temperature increases through T_c this magnetization vanishes. From equations 2.5 and 2.8 it is possible to obtain the following expression

$$M = \frac{Ng\mu_0(J+1)X}{3} = \frac{XkT}{g\mu_0 J\gamma}$$

where it has been assumed that $X << 1$. By taking the

derivative with respect to X of both sides of the above equation and evaluating it at $T = T_c$ and $X = 0$ it is possible to obtain the following relation between the Curie temperature and the Weiss constant.

$$T_c = \frac{N g^2 \mu_B^2 J(J+1)\gamma}{3k} \tag{2.9}$$

Let us now consider a temperature region above T_c so that there is no spontaneous magnetization. Then equation 2.5 becomes

$$M = \frac{N g^2 \mu_B^2 J(J+1)}{3kT} (H + \gamma M) \tag{2.10}$$

By using equations 2.9 and 2.10 it is possible to obtain

$$\chi = \frac{C}{T - T_c} \tag{2.11}$$

where $C = T_c/\gamma$. Equation 2.11 is known as the Curie-Weiss law.

This is a very successful phenomenological theory which describes accurately the results of many experiments. In deriving it Weiss made no attempt to explain the origin of the molecular field.

Heisenberg-Dirac theory of ferromagnetism

Heisenberg was the first to show that the Weiss local field could be given a quantum mechanical origin. This can be demonstrated by considering the Heitler-London

solution for a hydrogen molecule. Consider a simple system of two atoms, a and b, that have one electron each and are separated by a distance r_{ab}. See Figure 4.

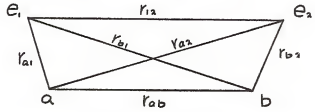

Figure 4. Hydrogen molecule.

Consider the following Hamiltonian.

$$H = T_1 - \frac{e^2}{r_{a1}} + T_2 - \frac{e^2}{r_{b2}} + \frac{e^2}{r_{ab}} + \frac{e^2}{r_{12}} - \frac{e^2}{r_{a2}} - \frac{e^2}{r_{b1}} \qquad (2.12)$$

where T denotes the kinetic energy operator and the subscripts identify the electrons. Consider also the following relationships.

$$\left(T_1 - \frac{e^2}{r_{a1}}\right)|a_{(1)}\rangle = \epsilon\,|a_{(1)}\rangle$$

$$\left(T_2 - \frac{e^2}{r_{b2}}\right)|b_{(2)}\rangle = \epsilon\,|b_{(2)}\rangle$$

$$\left(T_1 - \frac{e^2}{r_{b1}}\right)|b_{(1)}\rangle = \epsilon\,|b_{(1)}\rangle$$

$$\left(T_2 - \frac{e^2}{r_{a2}}\right)|a_{(2)}\rangle = \epsilon\,|a_{(2)}\rangle$$

where, for example, $|a_{(1)}\rangle$ denotes the atomic wave function for proton a and electron 1.

With the above wave functions it is possible to construct symmetric and antisymmetric wave functions for the system.

$$|S\rangle = \frac{1}{\sqrt{2}}\{|a_{(1)}b_{(2)}\rangle + |b_{(1)}a_{(2)}\rangle\}$$

$$|A\rangle = \frac{1}{\sqrt{2}}\{|a_{(1)}b_{(2)}\rangle - |b_{(1)}a_{(2)}\rangle\}$$

The functions $|a\rangle$ and $|b\rangle$ are not orthogonal. Define the overlap of these functions as $L \equiv \langle a|b\rangle$. With this and the assumption that the atomic wave functions are normalized it is possible to obtain the following.

$$\langle S|S\rangle = 1+L^2, \quad \langle A|A\rangle = 1-L^2 \qquad \langle S|A\rangle = 0$$

If the spin is considered it can be seen that there will be one antisymmetric spin wave function and three symmetric spin wave functions.

$$|a\rangle = \frac{1}{\sqrt{2}}\left(\eta_{1(+)}\eta_{2(-)} - \eta_{1(-)}\eta_{2(+)}\right)$$

$$|s\rangle = \frac{1}{\sqrt{2}}\begin{Bmatrix} \eta_{1(+)}\eta_{2(+)} \\ \eta_{1(+)}\eta_{2(-)} + \eta_{2(+)}\eta_{1(-)} \\ \eta_{1(-)}\eta_{2(-)} \end{Bmatrix}$$

where η is the spin function. The subscript identifies the electron and + or - denotes spin up or spin down. The simultaneous wave function must be antisymmetric. There are then the singlet state, $|Sa\rangle$, and the triplet state $|As\rangle$. The singlet state has spins paired and therefore no net magnetic moment. The triplet state is in

every way identical to a spin one particle with $M_z = 1, 0, -1$.

By forming $\langle \mathcal{S}|H|\mathcal{S}\rangle$ it is possible to obtain the energy shift for the singlet state

$$E_1 = 2\epsilon + \frac{K_1 + J_1}{1 + L^2}$$

where

$$K_1 = \langle b(2)\, a(1) | \frac{e^2}{r_{ab}} + \frac{e^2}{r_{12}} - \frac{e^2}{r_{1b}} - \frac{e^2}{r_{2a}} | a(1)\, b(2)\rangle$$

and

$$J_1 = \langle b(2)\, a(1) | \frac{e^2}{r_{ab}} + \frac{e^2}{r_{12}} - \frac{e^2}{r_{1a}} - \frac{e^2}{r_{2b}} | b(1)\, a(2)\rangle$$

K_1 represents the total electrostatic energy of the two atoms and J_1 is the exchange integral. From $\langle A|H|A\rangle$ it follows that the energy shift for the triplet state is

$$E_3 = 2\epsilon + \frac{K_1 - J_1}{1 - L^2}$$

Next, consider the energy difference between the singlet and the triplet state.

$$E_1 - E_3 = \Delta E = \frac{2(J_1 - L^2 K_1)}{1 - L^4} \equiv 2\mathcal{J}$$

If $\mathcal{J} > 0$ then the triplet state is energetically stable and the molecule will be magnetic.

Let

$$E_c = 2\epsilon + \frac{K_1 - L^2 J}{1 - L^2}$$

Using this, it is possible to write

$$E_1 = E_c + g \qquad E_3 = E_c - g$$

The total spin is a constant of the motion.

$$S^2 |Sa\rangle = S(S+1)\hbar^2 |Sa\rangle = 0$$

$$S^2 |A_\alpha\rangle = S(S+1)\hbar^2 |A_\alpha\rangle = 2\hbar^2 |A_\alpha\rangle$$

S_1^2 and S_2^2 are also constants of the motion with eigenvalues $\frac{3}{4}\hbar^2$. For the singlet state it can be shown that

$$\vec{S}_1 \cdot \vec{S}_2 |a\rangle = -\frac{3}{4}\hbar^2 |a\rangle$$

and for the triplet state one obtains

$$\vec{S}_1 \cdot \vec{S}_2 |\alpha\rangle = \frac{1}{4}\hbar^2 |\alpha\rangle$$

Consider the spin Hamiltonian,

$$H = E_c - \tfrac{1}{2} g - 2g \vec{S}_1 \cdot \vec{S}_2$$

It can be seen that it has the same eigenvalues as the electrostatic Hamiltonian used in the original formulation of the problem. This gives a spin-spin interaction with

a weight factor J that arises from electrostatic forces and symmetry requirements. This part of the Hamiltonian is called the Dirac-Heisenberg Hamiltonian.

$$H = -2 J_{ij} \vec{S}_i \cdot \vec{S}_j \tag{2.13}$$

One can now give an approximate connection between the exchange integral and the Weiss constant.[45] The assumption is often made that $J = 0$ for all atoms except the nearest neighbors and that $J = J_e$ for all neighboring pairs. Based on this

$$W_{ex} = -2 J_e \sum_{j} \vec{S}_i \cdot \vec{S}_j$$

where j indicates that the sum is to be taken only over nearest neighbors. Assume that the instantaneous values of the neighboring spins can be replaced by their time averages. Then

$$W_{ex} = -2 z J_e \left(S_{xi} \langle S_{xj} \rangle + S_{yi} \langle S_{yj} \rangle + S_{zi} \langle S_{zj} \rangle \right)$$

where z is the number of nearest neighbors. If the magnetization is along the z-axis then $\langle S_{xj} \rangle = \langle S_{yj} \rangle = 0$ and

$$W_{ex} = -\frac{2 z J_e S_{zi} M}{g \mu_B N} \tag{2.14}$$

This energy should equal the potential energy, V, of the spin i in the Weiss field γM.

$$V = -\gamma M g S_{zi} \mu_\beta \qquad (2.15)$$

Thus

$$\gamma = \frac{2z\mathcal{J}_e}{Ng^2\mu_\beta^2}$$

Using this and equation 2.9 it is possible to write

$$T_c = \frac{2z\mathcal{J}_e S(S+1)}{3k} \qquad (2.16)$$

Néel theory of antiferromagnetism

The Heisenberg theory of ferromagnetism is based upon the assumption that $\mathcal{J} > 0$. When $\mathcal{J} < 0$ an antiparallel arrangement of spins is favored and an antiferromagnetic substance is obtained. This type of system was investigated by Néel,[59] Bitter,[60] and Van Vleck,[61] and their work forms the foundation for the theory of antiferromagnetism.

Consider two interpenetrating lattices made up of sites A, with plus spins, and B, with minus spins. Assume that there are antiferromagnetic AA, AB, and BB interactions. Call these interactions w_{aa}, w_{ab} and w_{bb} respectively. Since A and B are symmetrical $w_{aa}=w_{bb}=\alpha$ and $w_{ab}=w_{ba}=\beta$. The effective fields can then be written

$$\vec{H}_{eff\,a} = \vec{H} - \alpha \vec{M}_a - \beta \vec{M}_b \qquad (2.17)$$

$$\vec{H}_{eff\,b} = \vec{H} - \beta \vec{M}_a - \alpha \vec{M}_b \qquad (2.18)$$

where $\vec{H}$ is the applied field and α and β are positive Weiss constants.

Following the same methods used in the Weiss theory one can write that in the limit of high temperature and small χ

$$\vec{M}_a = \frac{Ng^2\mu_B^2 J(J+1)}{3kT} \vec{H}_{eff\,a} \qquad (2.19)$$

where N is the number of A atoms per unit volume. Similarly, if the dipoles on B are identical to the ones on A then

$$\vec{M}_b = \frac{Ng^2\mu_B^2 J(J+1)}{3kT} \vec{H}_{eff\,b} \qquad (2.20)$$

Use equations 2.17-2.20 to obtain

$$\vec{M} = \frac{Ng^2\mu_B^2 J(J+1)}{3kT} \left[2\vec{H} - (\alpha+\beta)\vec{M}\right]$$

This becomes a scalar equation with the assumption that $\vec{M}$ and $\vec{H}$ are in the same direction.

$$\chi = \frac{M}{H} = \frac{2Ng^2\mu_B^2 J(J+1)/3k}{1 + N(\alpha+\beta)g^2\mu_B^2 J(J+1)/3k} = \frac{C}{T+\Theta} \qquad (2.21)$$

This is quite similar to the result obtained for the Weiss formulation of magnetism.

Next, examine the behavior at $T = T_N$. This temperature is still far enough away from saturation to use equations 2.19 and 2.20. With $H = 0$ write

$$\vec{M}_a = -\frac{N\mu^2}{3kT_N}(\alpha \vec{M}_a + \beta \vec{M}_b) \tag{2.22}$$

and

$$\vec{M}_b = -\frac{N\mu^2}{3kT_N}(\beta \vec{M}_a + \alpha \vec{M}_b) \tag{2.23}$$

where μ is the magnetic moment per atom, $\mu^2 = g^2\mu_B^2 J(J+1)$. From these it follows that

$$T_N = \frac{C}{2}(\beta - \alpha) \tag{2.24}$$

Observe that T_N increases as the interaction AB increases and decreases as AA and BB increases. A relationship can now be established between T_N and θ by using equations 2.21 and 2.24.

$$\frac{T_N}{\theta} = \frac{\beta - \alpha}{\beta + \alpha} \tag{2.25}$$

Experimentally it is found that $T_N < \theta$ which implies that $\alpha > 0$ or that, indeed, there is an antiferromagnetic AA and BB interaction.

Phenomenological discussion of ordering in heavy rare earths

Equations describing the types of ordering shown in Figure 2 may be written in the following form.

$$\mu_n^x = g\mu_B J M \cos(\vec{q}\cdot\vec{R}_n) \tag{2.26}$$

$$\mu_n^y = g\mu_B J M \sin(\vec{q}\cdot\vec{R}_n) \tag{2.27}$$

$$\mu_n^z = g\mu_B J M' \sin(\vec{q}\cdot\vec{R}_n+\delta) \tag{2.28}$$

where the z-axis is taken along the crystallographic c-axis and μ_n^x, μ_n^y, μ_n^z are the components of the moments on an atom at $\vec{R}_n$. M is, in this case, the relative saturation along both the x and the y axes and M' is the relative saturation along the z-axis. The vector $\vec{q}$ is parallel to the c-axis and has a magnitude, $\vec{q} = 2\pi/cd$, where d gives the period of the magnetic structure.

Equations 2.26 and 2.27, taken together, describe a helical structure while equation 2.28 alone describes a longitudinal wave structure. More complicated structures occur and may be described by variations of the above equations.

Next, examine the results obtained from a Heisenberg-Dirac form for the Hamiltonian.

$$H = -2\mathcal{J}(\vec{R}_n - \vec{R}_m)\,\vec{S}_n \cdot \vec{S}_m \qquad (2.29)$$

Since this exchange energy is, for the rare earths, usually much smaller than the splitting of the J multiplets by the spin-orbit coupling, De Gennes[62] has proposed that $\vec{S}$ for each atom must be projected on the total momentum J.

$$\vec{S} = (g-1)\,\vec{J} \qquad (2.30)$$

This comes from a phenomenological approach and has been examined and shown to be valid by several workers.[63,64] Using this expression and the above Hamiltonian one can obtain the exchange energy for the helical ordering described by equations 2.26 and 2.27.

$$E_{ex} = -2\mathcal{J}(\vec{q})\,N(g-1)^2 J^2 M^2 \qquad (2.31)$$

where

$$\mathcal{J}(\vec{q}) = \sum_{R_n} \mathcal{J}(R_n - R_m)\cos\left[\vec{q}\cdot(R_n - R_m)\right] \qquad (2.32)$$

For the longitudinal wave the exchange energy is

$$E_{ex} = -\mathcal{J}(\vec{q})\,N(g-1)^2 J^2 M'^2 \qquad (2.33)$$

where N is the number of atoms in the crystal.

Note that these structures are energetically most stable at that $\vec{q}$ which makes $\mathcal{J}(\vec{q})$ a maximum. Also, the spiral state is energetically more stable than the

longitudinal wave due to the factor of 2 found in the exchange energy of the former. However, in considering stable arrangements it is necessary to look at the free energy, $F = U - TS$. A molecular field approximation gives the same transition temperature for both structures.[65,66,67] This transition temperature can be written as $T_N = 2\,\zeta(\tfrac{7}{2})(g-1)^2 J(J+1)/3k$. One must look to the anisotropy energy to determine the relative stability of the structures.

Anisotropy

The term magnetic anisotropy refers to the dependence of the internal energy of a crystal on the direction of the spontaneous magnetization. The energy associated with this directional dependence is called the magnetic anisotropy energy. The dominant source of anisotropy in the rare earths is the electrostatic interaction between the multipole moments of the 4f electrons and the crystalline electric field. The crystalline potential for a hexagonal close pack structure takes the form[68]

$$\begin{aligned} V = {} & A_2^0 \textstyle\sum (3z^2 - r^2) + A_4^0 \sum (35z^4 - 30r^2z^2 + 3r^4) \\ & + A_6^0 \textstyle\sum (231z^6 - 315r^2z^4 + 105r^4z^2 - 5r^6) \\ & + A_6^6 \textstyle\sum (x^6 - 15x^4y^2 + 15x^2y^4 - y^6) \end{aligned} \qquad (2.34)$$

where A_n^m are the constants determined by the distribution of charges around the ions and z is taken along the c - axis. The summation is over the coordinates of all

of the electrons. This can be transformed into a more convenient form by use of the Wigner-Eckert theorem,[69]

$$
\begin{aligned}
H_a = {} & \alpha A_2^0 \langle r^2 \rangle \left[3J_z^2 - J(J+1) \right] \\
& + \beta A_4^0 \langle r^4 \rangle \left[35 J_z^4 - 30 J_z^2 J(J+1) + 3J^2(J+1)^2 + 25 J_z^2 - 6J(J+1) \right] \\
& + \gamma A_6^0 \langle r^6 \rangle \left[231 J_z^6 - 315 J(J+1) J_z^4 + 105 J^2 (J+1)^2 J_z^2 - 5 J^3 (J+1)^3 \right. \\
& \left. + 735 J_z^4 - 525 J(J+1) J_z^2 + 40 J^2 (J+1)^2 + 294 J_z^2 - 60 J(J+1) \right] \\
& + \gamma A_6^6 \langle r^6 \rangle \tfrac{1}{2} \left[(J_x + i J_y)^6 + (J_x - i J_y)^6 \right]
\end{aligned}
\qquad (2.35)
$$

where α and β are constants which have been evaluated by Stevens. The $\langle r^n \rangle$ are the mean values of r^n over the 4f electron distribution and may be computed.[70] The A_n^m are very difficult to evaluate and only order of magnitude estimates have been obtained.[71]

If H_a is treated as a perturbation on H_{ex}, it is found that at high temperatures the first term is the dominant one, but at low temperatures the higher order terms also become important. The first term corresponds to the quadrupole moment and causes the preferred direction of the ordered moment to be either $\perp$ or $\parallel$ to the c-axis depending upon whether α is positive or negative. The second and third terms cause the moments to tend to align parallel to c when they are negative, but when they are positive the preferred direction is at an angle from c.

For dysprosium and terbium the first term is dominant and is negative over the whole ordered range. The ferromagnetic transition in these elements is caused by an increase in the fourth term with decreasing temperature. For erbium the third term is positive and fairly large and makes the conical structure stable at low temperatures.

This method of combining an exchange interaction with crystal anisotropy has given very good qualitative results. As yet no quantative calculations have been made due to the extreme complexity of the problem.

Range of exchange interaction

In order to obtain some idea of the range of the exchange interaction necessary to stabilize the screw structure we look at a particular model.[72] Assume that the exchange interaction, J , between layers of atoms perpendicular to the c-axis extends as far as second-neighbor layers. The exchange Hamiltonian now takes the form

$$H_{ex} = -\sum_{i} \sum_{n=0,\pm 1,+2} 2J_n \vec{S}_i \cdot \vec{S}_{i+n}$$

where $\vec{S}_i$ is the average spin of an atom in the ith layer. By summing this exchange Hamiltonian it is possible to obtain an expression for the exchange energy. By referring back to equation 2.31 it is possible to see that

the assumed spiral configuration will be made most stable by the values of $\vec{q}$ that maximize $J(\vec{q})$. The $J(\vec{q})$ for this model can be written

$$J(\vec{q}) = J_0 + 2J_1 \cos\frac{qc}{2} + 2J_2 \cos qc .$$

The value of q which maximizes this expression is

$$\cos\frac{qc}{2} = -\frac{J_1}{4J_2} .$$

An analysis of the available data for dysprosium has been made by Enz[72] and the values $J_0/k = -24$, $J_1/k = 44$ and $J_2/k = -15$ obtained. Similar results were obtained from an analysis of data on erbium. Observe that $J(R)$ is rapidly oscillating and long ranged to produce this spiral structure. Since the overlap of the 4f electrons on neighboring atoms must be quite small it would seem that this long range interaction is due to some other effect. It is reasonable to consider that the main part of the exchange interaction is produced by the exchange coupling between the conduction electrons and the localized spins.

Indirect exchange

Indirect exchange has been extensively investigated;[73,74,75] the following discussion closely follows that of Liu.[76] He starts by considering one conduction electron interacting with the magnetic electrons of one ion. The interaction Hamiltonian can be written as

$$H_I = \sum_{i=1}^{N} \frac{e^2}{|\vec{r}_i - \vec{r}_{n+1}|} \tag{2.36}$$

where $\vec{r}_{n+1}$ is the position of the conduction electron and $\vec{r}_i$ is the position of the ith magnetic electron. The wave function for the conduction electron is of the form

$$\Psi(\vec{r},s) = \mu_k(\vec{r}) \exp\{i\vec{k}\cdot\vec{r}\}\ \eta \tag{2.37}$$

where

$$\mu_k(\vec{r}) \exp\{i\vec{k}\cdot\vec{r}\}$$

is a Block function and η is the Pauli spin function. Since the 4f electrons are well shielded their wave function can be written in the form

$$\Psi_{l\mu}(\vec{r})\,\eta = R(\vec{r})\,Y_{l\mu}(\theta,\phi)\,\eta \tag{2.38}$$

The wave function for the entire shell is constructed from the single particle wave function as prescribed by Hund's rules and the Pauli exclusion principle. Since this dissertation deals only with dysprosium and erbium, for which the 4f shell is over half full, only that case will be considered.

Liu[76] showed that the required wave function of the shell is

$$\Psi_{JM} = \sum_{m,t} C(LSJ;\, m, M-m)\, A_{mt}\, \Psi_{L\,m,t}\, \Psi_{S,M-m,t} \tag{2.39}$$

where $C(LSJ;m,M-m)$ denotes the vector coupling coefficient and the summation over t refers to a summation over Young's diagrams.[77]

The wave function of one conduction electron and one magnetic shell with no regard to symmetry is

$$\Psi = \Psi_{JM}(1,\ldots,N)\,\Psi_{(N+1)} \tag{2.40}$$

where $\Psi_{(N+1)} = \Psi(\vec{r}_{N+1}, s_{N+1})$. Next, this wave function must be antisymmetrized with respect to all the $N+1$ particles. The resulting wave function is

$$\Psi = \frac{1}{(N+1)^{1/2}}\left[\Psi_{JM}(1,\ldots,N)\,\Psi_{(N+1)} - \sum_{i=1}^{N} \Psi_{JM}(1,\ldots,i-1,N+1,i+1,\ldots N)\,\Psi_{(i)}\right] \tag{2.41}$$

The particles are considered to be completely indistinguishable; therefore equation 2.36 must be symmetrized.

$$H_I = \sum_{i>j} \frac{e^2}{|\vec{r}_i - \vec{r}_j|} \tag{2.42}$$

where $i \geq 1$, $j \leq N+1$ and $i \neq j$. Consider the following unsymmetrized initial and final states.

$$\Psi_i = \Psi_{JM}(1,\ldots,N)\,\Psi_{(N+1)} \tag{2.43}$$

$$\Psi_f = \Psi_{JM'}(1,\ldots,N)\,\Psi'_{(N+1)} \tag{2.44}$$

where

$$\Psi_{(N+1)} = u_k(\vec{r}_{N+1})\,\exp\{i\vec{k}\cdot\vec{r}_{N+1}\}\,\eta$$

$$\Psi'_{(N+1)} = u_{k'}(\vec{r}_{N+1})\,\exp\{i\vec{k}'\cdot\vec{r}_{N+1}\}\,\eta'$$

Using the expression for Ψ_{JM} , equation 2.39, one can now form the matrix elements of the exchange interaction, $\langle \Psi_f | H_{ex} | \Psi_i \rangle$.

Liu obtains an expression for H_{ex} for the heavy rare earths which includes direct interaction between shell electrons, exchange interaction between shell electrons, direct interaction between conduction and shell electrons and exchange interaction between conduction and shell electrons. The last of these is found to be

$$H = -2\, I_{(k,k')}(g-1)\, \vec{s}\cdot\vec{J} \qquad (2.45)$$

where $I_{(k,k')}$ is the exchange integral, $\vec{s}$ is the spin of the conduction electron and $\vec{J}$ is total angular momentum of the ion. In order to obtain equation 2.45 Liu made the following approximations. 1) The conduction electrons are s electrons so their wave functions have spherical symmetry. 2) The wavelength of the conduction electron is large compared with the size of the 4f shell so that $exp\{i\vec{k}\cdot\vec{r}\}$ may be approximated by the leading term of its power series expansion.

It is very difficult to justify the first approximation and Liu did not try to show that it held. The second one can be examined by looking at the radius of the 4f shell as determined by the method of Pauling.[78] It is

found to be about 0.4 A. Using the free electron approximation it is found that, for the heavy rare earths, $k \simeq 1.5 \times 10^8$ cm^{-1} at the Fermi energy. Therefore, $\vec{k} \cdot \vec{r} \approx 0.6$, and the second approximation is seen to be reasonable.

Recently Kaplan and Lyons[73] have examined this second approximation and found that the leading term does indeed dominate for terbium through erbium and that the correction by other terms is about 10 per cent.

De Gennes[62] has found that since $I(k,k')$ should be the same for all rare earths T_c or T_N should be proportional to $(g-1)^2 J(J+1)$. For the heavy rare earths this reduces to $S^2(J+1)/J$. This is the same result that Néel obtained in 1938[79] based on the molecular field approximation. This relationship is verified experimentally except for ytterbium.

Pressure effects

Using an equation first derived by Néel, Robinson et al.[39] have constructed an interaction curve for the rare earths in an attempt to predict the effect of pressure on the transition temperatures. The Néel equation is

$$\frac{J_c}{k} = \frac{3\Theta_c J}{2 z S^2 (J+1)} \qquad (2.46)$$

where Θ_c is the transition temperature and z is the number of nearest neighbors. Using known values of the

right hand side of this equation the quantity $\mathcal{J}_e/k$ was calculated and plotted versus $D/2R$ where D is the interatomic spacing and R is the radius of the 4f shell. There is some difficulty in using θ_c in equation 2.46 for the rare earths. In materials which go directly from the paramagnetic to the ferromagnetic state θ_{cf}, the temperature at which the material actually becomes ferromagnetic, is a few per cent lower than θ_{cp}, the extrapolated transition temperature, so it makes little difference which is used. In the heavy rare earths where antiferromagnetic states are observed these two temperatures are far apart. To account for this, two curves were plotted, one based on θ_{cf} and one on θ_{cp}. The resulting curve is shown in Figure 22., This analysis accounts for the magnitude and sign of the dT_c/dP found for gadolinium and terbium and can be used to explain their result that dT_c/dP for dysprosium is positive for low pressures and changes to negative as the pressure is increased.

Liu has done an analysis of the effect of pressure on T_c for ferromagnetic materials.[80] He has looked specifically at gadolinium but was able to draw conclusions about the behavior of heavy rare earths from his work. The starting point chosen for this analysis is the indirect exchange Hamiltonian

$$H = \sum_i \frac{p_i^2}{2m^*} + \sum_i I(\vec{r}_i - \vec{R}_i)\ \vec{s}_i \cdot \vec{S}_i \qquad (2.47)$$

where the first term is the kinetic energy of the conduction electrons in the scalar effective mass approximation and the second is the exchange interaction between the conduction electrons and the ions. The subscript i refers to the conduction electrons while j refers to the ions. As in the previous discussion of the indirect exchange the electron is described by a Block function. The matrix elements of equation 2.47 are written as

$$\frac{1}{N}\,\vec{s}_i\cdot\vec{S}_j\,I_{kk'}\exp\{i(\vec{k}-\vec{k}')\cdot\vec{R}_j\}$$

where

$$I_{kk'}=N\int\varphi^{*}_{k'}(\vec{r})\;I(\vec{r})\;\varphi_k(\vec{r})\,d\vec{r}$$

It has been shown[81,74,75] that by second order perturbation theory the exchange interaction can be expressed by the spin Hamiltonian

$$H_s=\sum_{i\neq j}\sum_{j}J(\vec{R}_{ij})\,\vec{s}_i\cdot\vec{S}_j \qquad (2.48)$$

with

$$J(\vec{R})=\frac{|I|^2\,m^{*}V^2}{4N^2\,(2\pi)^3\,\hbar^2R^4}\left[2k_fR\cos(2k_fR)-\sin(2k_fR)\right] \qquad (2.49)$$

where I^2 is the average matrix element for k and k' approximately equal to k_f. Equation 2.49 can alternately be written as

$$J(\vec{R})=\frac{3\pi z}{4N}|I|^2\,N(\epsilon_F)\,F(2k_fR) \qquad (2.50)$$

where Z is the valence of the ion, $N(\epsilon_F)$ is the density of states at the Fermi level and $F(x)$ is given by

$$F(x) = \frac{x\cos x - \sin x}{x^4}$$

De Gennes[62] has shown that it is reasonable to assume that the ferromagnetic state is the ground state for gadolinium. Following this we can write

$$E_g = \frac{3\pi z}{4} |I|^2 S^2 N(\epsilon_F) \sum_i F(2k_F R_i) \qquad (2.51)$$

This equation should now be examined for terms which will vary with pressure. The summation will be independent of volume if the electron distribution is isotropic. The Z and S are independent of volume in the heavy rare earths. One can now take the logarithm of equation 2.51 and form

$$\frac{\partial \ln E}{\partial \ln V} = \frac{\partial \ln |I|^2}{\partial \ln V} + \frac{\partial \ln N(\epsilon_F)}{\partial \ln V} \qquad (2.52)$$

The Curie temperature is proportional to the ordering energy per spin, therefore we may write

$$\frac{\partial \ln T_c}{\partial \ln V} = \frac{\partial \ln |I|^2}{\partial \ln V} + \frac{\partial \ln N(\epsilon_F)}{\partial \ln V} \qquad (2.53)$$

The terms on the right side of equation 2.53 are unknown at the present time. Liu gives some estimates of the limits that can be expected for them. The thing that should be noted about them is that they are both functions only of the electronic properties of the material. Since

all of the heavy rare earths have similar electronic properties, $\frac{\partial \ln T_c}{\partial \ln V}$ should be the same for each. This is a rather strong assumption and should be subjected to experimental verification. This is discussed further in Chapter IV.

Thermodynamics of phase transitions

It is generally accepted that the transition from the paramagnetic to the antiferromagnetic state is second order while the transition from the antiferromagnetic state to the ferromagnetic state is first order.[52]

It is possible to characterize a first order phase transition by either of the following statements.[82] 1. There are changes of entropy and volume. 2. The first order derivatives of the Gibbs function change discontinuously. Any phase transition that satisfies these requirements is known as a phase change of the first order.

The effect of pressure on a first order phase transition can be determined simply by taking the first Tds equation of thermodynamics and integrating it over the change of phase. The first Tds equation can be written,

$$Tds = c_v dT + \left(\frac{\partial P}{\partial T}\right)_v dv \qquad (2.54)$$

Integrating this it is possible that one obtains,

$$\frac{dT}{dP} = \frac{v^f - v^i}{s^f - s^i} \tag{2.55}$$

In this equation the superscript f refers to the final phase and i refers to the initial phase.

A second order phase transition is characterized by discontinuous changes in the second order derivatives of the Gibbs function. There is no change in entropy associated with this transition. Using the same superscipt notation as before it is possible to write $s^i = s^f$ at (T, P) and $s^i + ds^i = s^f + ds^f$ at $(T+dT, P+dP)$. These expressions yield

$$T ds^i = T ds^f \tag{2.56}$$

The second TdS equation is now used,

$$T ds = c_p dT - \left(\frac{\partial v}{\partial T}\right)_p dP$$

By using equation 2.56 and the definition of the volume expansivity

$$\beta = \frac{1}{v}\left(\frac{\partial v}{\partial T}\right)_p$$

it is possible to write

$$c_p^i dT - T v \beta^i dP = c_p^f dT - T v \beta^f dP$$

By re-arranging and using the relation $\beta = 3\alpha$ and $\rho = \frac{1}{v}$ one obtains

$$\frac{dT}{dP} = \frac{3T}{\rho} \frac{\Delta\alpha}{\Delta C} \tag{2.57}$$

where $\Delta\alpha = \alpha^f - \alpha^i$ and $\Delta C = C_p^f - C_p^i$. Equation 2.57 is known as an Ehrenfest equation. This equation predicts the pressure shift for the Néel transition and is further discussed in Chapter IV.

CHAPTER III

APPARATUS AND PROCEDURE

Introduction

A description of the apparatus and of the procedure involved in the measurements made in this dissertation can be roughly divided into four major sections. The first section is concerned with the detection of the ferromagnetic-antiferromagnetic and antiferromagnetic-paramagnetic phase transitions. This task is complicated by the fact that the sample is contained inside a pressure bomb which is in turn contained within a temperature control cryostat. Further complications arise from the safety requirement that every thing should be operated remotely. The second section deals with the techniques involved in the compression, containment and pressure measurement of helium gas at high pressures and low temperatures. The third section concerns the production and measurement of temperatures from 5°K to 190°K, and the last section gives a step-by-step breakdown of the procedure used in performing the experiments.

Detection of Magnetic Transitions

Several methods have been used to detect magnetic transitions in rare earths. The most important of these are neutron diffraction, bulk magnetic measurements, specific heat measurements and electron transport property measurements.

It was decided to look at the bulk magnetic properties in these experiments since they promised to give sensitive indications of the transitions, would readily lend themselves to pressure studies, and did not require any elaborate instrumentation. Methods of detection of the transitions by bulk magnetic properties are mentioned in Chapter I. Several factors had to be considered in deciding upon the proper method to be used. It was desired to have as much sensitivity as possible; therefore a bridge method was selected. A large filling factor was desirable so the coil was placed inside of the bomb. Since the working space was limited and since the number of electrical leads into the high-pressure region should be minimized, it was decided to use a single coil technique. After the experiments were well under way Samara and Giardini[37] reported that they had used the same method. The sample, in the form of a cylinder, was placed within a solenoid and the self-inductance of the coil was monitored. There is no simple exact formula for the self-inductance of a solenoidal coil of practical dimensions.

An approximate formula is

$$L \approx \frac{0.8\, a^2 n^2}{6a + 9b + 10c}$$

where a is the mean radius, b is the length, c is the radial thickness of the solenoid and n is the number of turns. The important thing to note is that L is proportional to μ, the permeability of the core material. As a ferromagnetic sample is heated through its Curie temperature, its permeability changes from a large to a fairly small number. Hence, if the inductance of the coil is monitored, a large drop is seen as the sample is heated through its Curie temperature. The transition from the antiferromagnetic to the paramagnetic state is accompanied by a peak in the permeability versus temperature curve. Of course, the inductance of the coil would also be a function of the thermal expansion of the copper wire and the sample, and of variations of μ due to skin effects. A blank run was made to insure that the changes in the coil were not influencing the results. Since the magnetic changes are quite large it was reasonable to neglect the other effects.[37]

Inductance bridge

In order to perform these experiments a very sensitive self-inductance bridge was needed. The design of inductance and capacitance bridges has been advanced considerably in recent years with the development of very

accurate ratio transformers.[83,84] These instruments utilize modern high permeability magnetic core materials and are highly accurate alternating voltage dividers.[85] A ratio transformer bridge was built following a design by Hillhouse and Kline.[86] This bridge was capable of detecting changes of inductance of the sample coil of one part per million.

The wiring diagram, Figure 5, shows the components as connected in the bridge. This design features the use of commercially available components as listed below:

1. Audio oscillator, Hewlett-Packard Model 200JR
2. Isolation transformer, Gertsch Model ratio 4-1
3. Ratio transformer, Gertsch Model 1011
4. Decade resistance box, General Radio Type 1432-K
5. Null detector, General Radio 1232-A
6. Standard inductor, General Radio 1482-L
7. Standard inductor, General Radio 1482-H

All of these components, except the null detector and the audio oscillator, are contained within one cabinet. Figure 6. All of the external wiring is coaxial cable (GR 874-R34) with General Radio shielded connectors. The switch, S_1, allows the isolation transformer to be connected with a ratio of 4:1 or 1:4. The 600 ohm generator output impedence can then be transformed to 37 ohms or 9000 ohms. The purpose for this approximate impedance matching was to

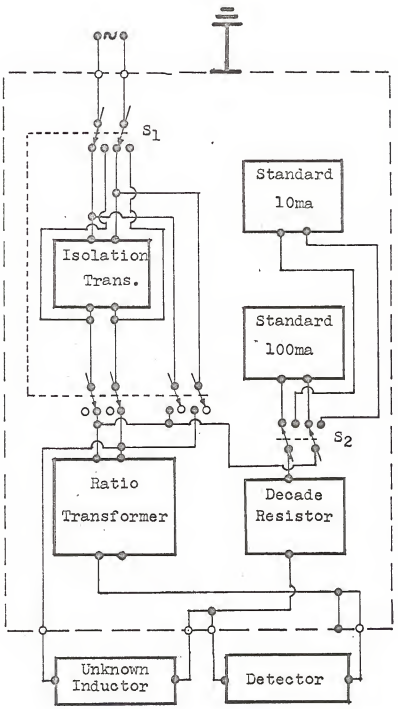

Figure 5. Wiring diagram for the inductance bridge.

Figure 6. Inductance Bridge.

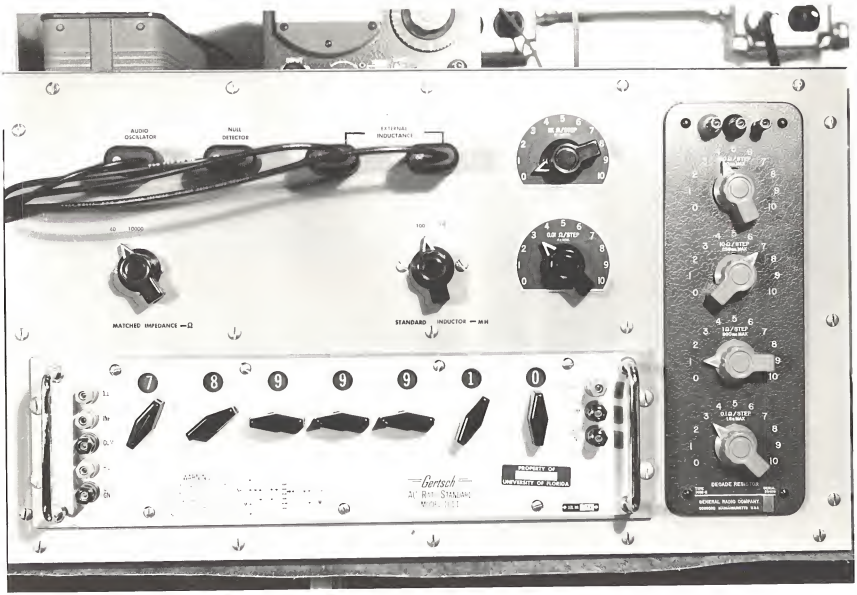
AUDIO OSCILLATOR
NULL DETECTOR
EXTERNAL INDUCTANCE
MATCHED IMPEDANCE — Ω
STANDARD INDUCTOR — MH
GENERAL RADIO COMPANY
DECADE RESISTOR
PROPERTY OF UNIVERSITY OF FLORIDA
Gertsch
AC RESISTANCE STANDARD

realize good bridge sensitivity. The ideal ratio between unknown inductance and standard inductance is 1:1; however, Hillhouse and Kline found that the accuracy was not appreciably altered up to a ratio of 10:1. Switch S_2 allows for the use of either the 10 mh or the 100 mh standard inductor. The equivalent circuit for the bridge is shown in Figure 7. The operating equations for the bridge are derived below. Standard notation is used with subscripts 1 and 2 referring to the leads running from the bridge to the sample coil, S, to the standard, D, to the decade resistance and X, to the sample coil. The reading on the ratio transformer, A , is that part of the total voltage that is being applied across the unknown inductor. Looking at the schematic it is seen that at the balanced condition, that is, when the current through the detector equals zero, one can write

$$e_1 = E(1-A) = I[R_1+R_S+R_D+j\omega(L_1+L_S+L_D)] \qquad (3.1)$$

$$e_2 = EA = I[R_X+R_2+j\omega(L_X+L_2)] \qquad (3.2)$$

Dividing equation 3.1 by equation 3.2 gives

$$(1-A)[R_X+R_2+j\omega(L_X+L_2)] = A[R_1+R_S+R_D+j\omega(L_1+L_S+L_D)] \qquad (3.3)$$

Thus

$$R_X = \frac{A}{1-A}(R_S+R_D+R_1) - R_2 \qquad (3.4)$$

and

$$L_x = \frac{A}{1-A}(L_s + L_D + L_1) - L_2 \qquad (3.5)$$

Equations 3.4 and 3.5 constitute the operating equations for the bridge.

The inductance of the decade resistor is given by the manufacturer and at the maximum is on the order of a μH. The inductance of leads 1 and 2 are also on the order of a μH. During an experimental run the transitions occur over a small temperature range; therefore L_D, L_1 and L_2 are small and essentially constant. The L_x is from 1/2 to 1 Henry and changes in it completely dominate the picture. The situation with the resistances is similar. R_1 and R_2 are small and essentially constant during the determination of the transition temperature. Using this information, one can truncate the operating equations and simplify data reduction. The simplified equations are:

$$R_x = \frac{A}{1-A}(R_s + R_D) \qquad (3.6)$$

$$L_x = \frac{A}{1-A} L_s \qquad (3.7)$$

Hillhouse and Kline have made a detailed error analysis for this bridge design and found that it is able to intercompare inductances at ratios as large as 10:1 to

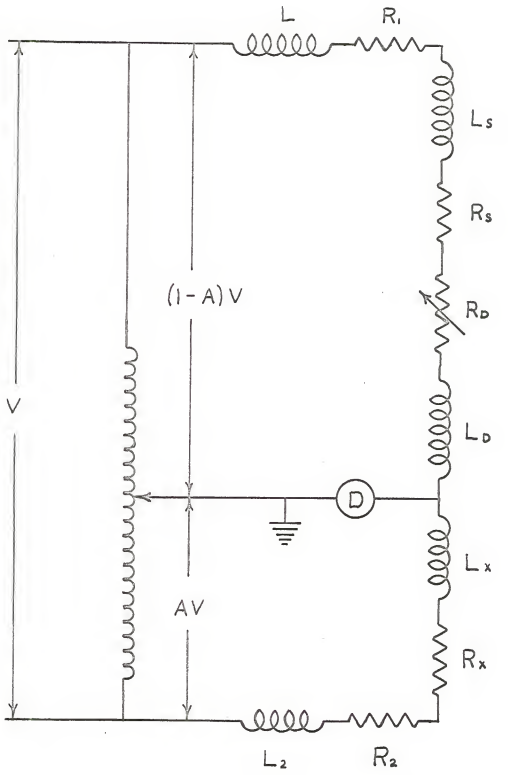

Figure 7. Equivalent circuit for the inductance bridge.

accuracies an order of magnitude better than the certification limits of present standards which is at best ±.03 per cent.

Coil and sample description

The two coils used in these experiments were wound on a teflon core with a Model W coil winder manufactured by the Coil Winding Equipment Company. The dimensions and room temperature characteristics are:

Table 3. Sample coils.

	Coil 1	Coil 2
Number of turns	14,000	17,000
Length	13/16 in.	13/16 in.
Inside diameter	1/8 in.	1/8 in.
Outside diameter	7/16 in.	1/2 in.
Resistance	3100 ohms	6000 ohms
Inductance	400 mH	500 mH

The samples were obtained from Leytess Metal and Chemical Corporation who specified a purity of 99.9 per cent. When received they were in the form of rods 6 in. long and .375 in. diameter. These were cut and turned down to a final sample size of 1/8 in. diameter by 13/16 in. long. The samples were not annealed after machining.

Pressure Generation and Measurement

The purpose of these experiments was to study the effect of hydrostatic pressure on magnetic transitions in rare earths. A large high pressure helium gas facility was constructed to achieve purely hydrostatic pressure over most of the temperature range covered. In principle, it is easy to achieve hydrostatic pressure in the fluid or gaseous phase of helium. In the lower temperature region approximately hydrostatic pressures may be achieved by applying the desired pressure to the helium while it is in the fluid phase and then freezing it at constant pressure. Further cooling necessitates the calculation of the pressure from the equation of state of solid helium and the thermal properties of the high-pressure bomb,[87] which was made of beryllium-copper. This procedure gives very nearly hydrostatic pressure even though there is some movement due to the fact that helium has a larger thermal expansion coefficient than beryllium-copper.

Numerous experimental difficulties arose during the course of the experiments. By far the largest problem was leaks in the pressure system. The bomb plug seals presented the most difficulty since a leak there made temperature determination and control impossible. Cooling through the freezing temperature of helium had to be done very carefully to prevent blocking of the inlet pressure line before the helium in the bomb was completely solidified.

This would have greatly reduced the pressure at the sample as well as the accuracy with which it was known.

High-pressure room

The safest way in which to conduct high pressure experiments is not to have any personnel in the vicinity of the high-pressure equipment. This was done by isolating all of the high-pressure components in a specially constructed, explosion proof room below ground level. This room was located outside the basement of the low temperature laboratory. All of the pressure equipment plus cryogenic apparatus was operated remotely from the adjoining basement. A brief description of this room will now be given.

Figure 8 shows an outside view of the room. The wall on the left is the outside wall of the Physics building basement. Figure 9 shows a top view of the room and part of the laboratory, giving wall details and rough dimensions. The roof of the room was constructed, from inside out, of 1/2 inch aluminum plate, 4 inches of sand, 9 inches of reinforced concrete, a 4 inch air gap, 1/2 inch plywood sheet, and a layer of sand bags resting on this plywood. Over this was placed another 1/2 inch plywood sheet which was covered with roll roofing. The outside end of the air gap was covered with screen and provided ventilation as well as a path for escaping gas in the event of an accident. The free volume of the compressed gas was only about one-

Figure 8. Entrance to high-pressure room.

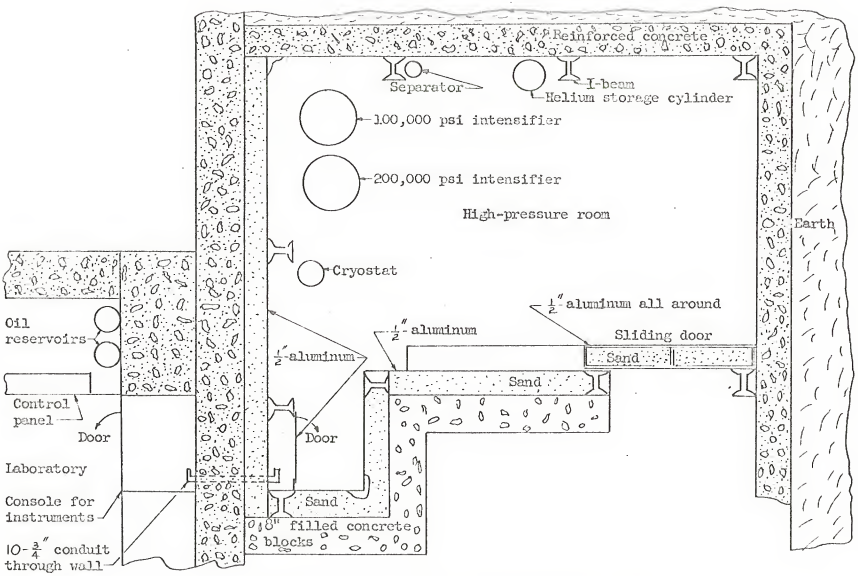

Figure 9. Top view of high-pressure room.

fortieth of the volume of the room and therefore could not create a significant increase in the pressure of the room. However, liquid nitrogen and helium dewars as well as the commercial helium gas tank were left in the room for remote transfer and if one of these should be ruptured by shrapnel it would release enough gas to be dangerous in a poorly vented room. The door was a 5 1/2 inch thick box made of 1/2 inch aluminum plate and filled with sand. The box was supported by a steel dolly which had 6 ball bearing steel wheels that rolled in the channel of a 6 inch steel I beam. The north and east walls of the room (Figure 8) consist of 12 inches of steel reinforced concrete backed by earth. The south wall was constructed, from inside out, of 1/2 inch aluminum plate, 6 inches of sand, and a wall of 8 inch solid concrete blocks. The west wall consists of the outside wall of the Physics building, 15 inches of reinforced concrete, supplemented by a 1/2 inch aluminum plate and 6 inches of sand. It was deemed necessary to add this plate and sand to prevent spalding of the concrete wall in the event shrapnel struck the wall.[88] The room was designed to contain all shrapnel and shock waves in the event of a high-pressure gas failure.

High-pressure gas apparatus

The high-pressure system is a three stage system composed of an Aminco 30,000 psi (H 5968) oil-to-gas

separator, a Harwood 100,000 psi intensifier (SA10-8-1.250-100K), and a Harwood 200,000 psi intensifier (SA10-6-.875-200K). Figure 10 is a schematic showing all of the significant components. Figure 11 shows the relative size and the placement of the components within the room.

Initial charging was accomplished by a remotely operated solenoid valve (switch located on the panel). For safety, a second solenoid valve was used to bleed the 2,000 psi stage of the gas system after charging. The charging gas flowed through a liquid nitrogen cold trap and a filter to remove gas and solid impurities. Note that each stage was separated from its lower pressure adjoining stage by a one way ball check valve, as shown in Figure 10. The check valves in the 30,000 psi stage were Aminco No. 44-6386 while the ones in the other stages were Harwood ML-603.

The Heise gauge, Model H 26960, located in the 100,000 psi stage, was monitored by a closed circuit television system which consists of a Marson television monitor and a Bell camera. This gauge proved very useful in locating leaks and controlling bleed down rates in the system. The pressure during an experiment was always measured with the Harwood manganin resistance cell. This pressure was monitored constantly by a Foxboro recorder but data points were taken with a Carey-Foster bridge.

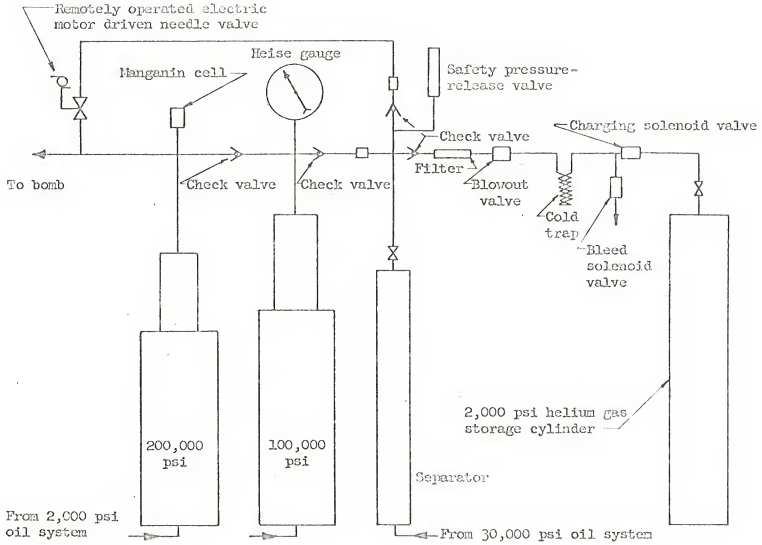

Figure 10. Schematic of high-pressure system.

Figure 11. Inside view of high-pressure room.

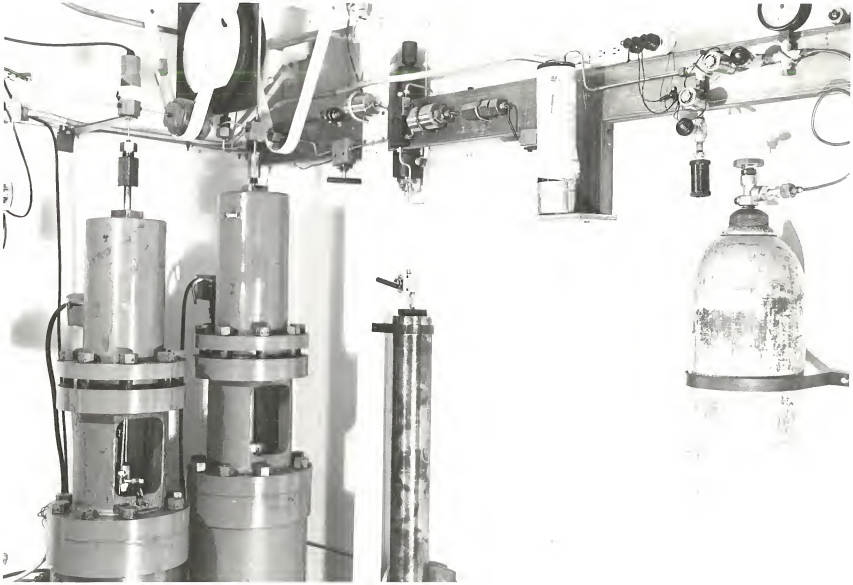

Harwood Manufacturing Company specifies an error of less than 1 per cent with this cell and bridge. The schematic also shows the motor driven bleed valve. This was a Harwood 200,000 psi needle valve driven by an electric motor through a chain and sprocket arrangement.

Control panel

Figure 12 is a schematic of the control panel and Figure 13 is a photograph of the actual panel. The schematic shows that the control panel was divided into two separate pumping systems; a 30,000 psi oil system for the gas-to-oil separator, and a 2,000 psi oil system for the two intensifiers. Sprague Engineering Corporation air powered pumps were used for both systems. As a safety feature the air supply was taken through a 115-volt ac solenoid valve that was normally closed. In the event of electrical power failure, affecting other components of the facility, the air supply was automatically stopped and had to be manually tripped on when power was restored. The intensifier oil system operated at reasonably low pressure so it was practical to use one pumping system with electrically coupled solenoid valves to draw oil from the proper reservoir and to direct it to the proper intensifier. These solenoid valves were operated by push button switches on the panel, and pilot lights indicated which reservoir the oil was taken from and the intensifier

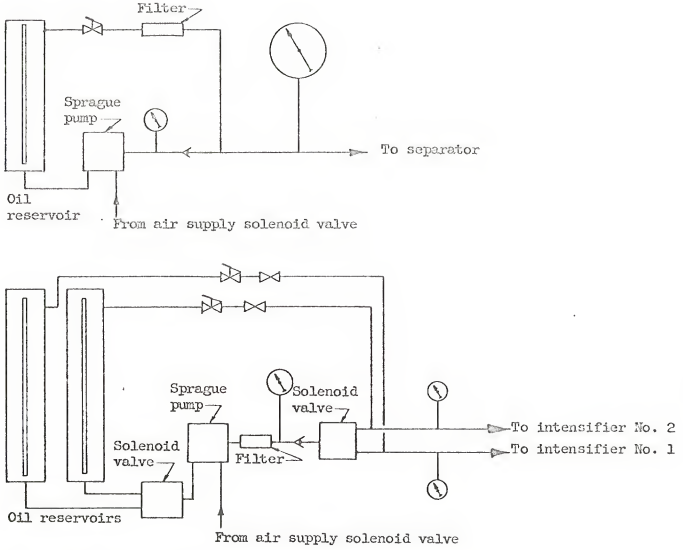

Figure 12. Schematic of the control panel for the pressure system.

Figure 13. Control panel.

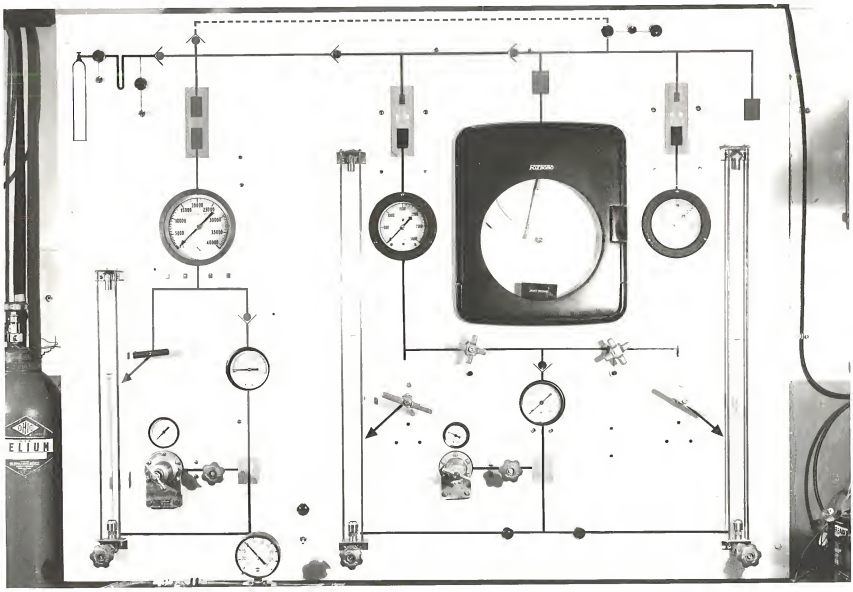
ELIUM

to which it was pumped. Each oil reservoir was fitted with a level indicating sight tube. These were calibrated to show the actual position of the appropriate piston in the high-pressure room. Stainless steel tube, type 304, with 3/8 inch OD was used throughout the intensifier system, while 30,000 psi Aminco high-pressure tubes and fittings were used in the separator system.

The photograph of the control panel (Figure 13) shows the position of the pumping controls. This panel was designed for maximum safety, efficiency, and convenience of operation. A color coded flow diagram was painted on the panel to clarify the oil and high-pressure gas circuits. Also shown on the panel is the Foxboro Dynalog recorder which was used to monitor continuously the Harwood manganin resistance cell located in the 200,000 psi gas stage. A Harwood Carey-Foster bridge (visible on the shelf in the lower right-hand corner of Figure 13) was used for accurate readings of this cell. Visual observations in the room were made with closed circuit television.

The push button and two warning lights in the upper left-hand corner of the control panel (Figure 13) remotely controlled the electric motor operated bleed valve in the 200,000 psi gas stage which bled this high pressure back into the 30,000 psi gas stage. A safety microswitch was located at the 30,000 psi stage oil reservoir which prevented operation of this motor unless the separator was

cycled all the way back, thereby providing adequate volume for the 200,000 psi gas.

High-pressure bomb

In high-pressure, low-temperature experiments conflicting design considerations occur with the sample container (bomb). The bomb should be massive and strong to safely hold the pressure yet it must be small with low thermal mass so that it will fit a cryostat of reasonable size and can be cooled to low temperatures without using an excessive amount of liquid helium. Further, it was planned to use this bomb for magnetic measurements and nuclear resonance work, so a non-magnetic material was required. The desire for a non-magnetic bomb with high strength led to the choice of BeCu (Berylco 25) for the bomb material.

A design pressure of 225,000 psi was used so that the bomb would be reasonably safe with the 200,000 psi gas system. Standard thick-wall cylinder equations[89] gave stresses exceeding the yield strength of full hard BeCu regardless of the wall ratio (outside diameter/inside diameter). These same equations, modified for a double wall cylinder,[89] predict sub yield point maximum stress for the dimensions shown in Figure 14. The outer cylinder was a .010-inch interference fit (on diameter) over the inner one. Assembly was accomplished by cooling the inner cylinder in

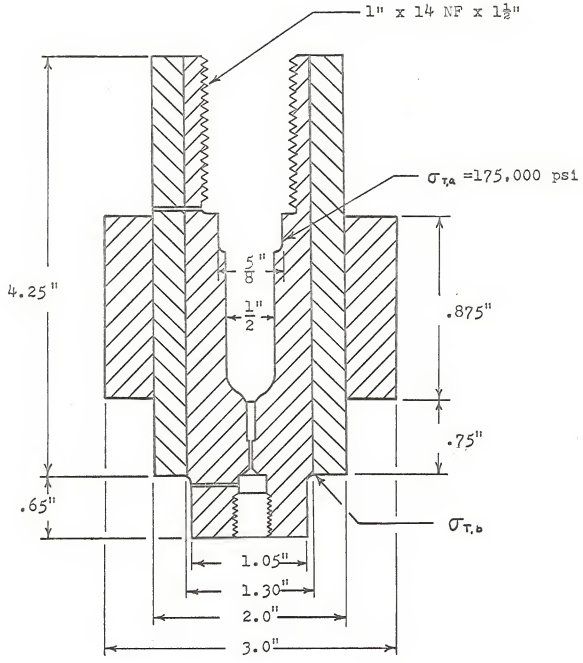

Figure 14. High-pressure gas bomb.

liquid nitrogen and heating the outer cylinder to 900°F, then pressing them together. The assembly was then heat treated at 600°F for 3 hours. Final machining on the inside bore and sealing surfaces was done after the outer cylinder was fitted. Figure 14 shows the finished bomb with dimensions and the tangential stress σ_T at the critical design points as calculated for an internal pressure of 225,000 psi. It was very important that all corners and edges be made round and smooth to reduce stress concentration.

Before use in the helium gas system, the bomb was pressurized with a liquid test system to 14 kilobars and carefully checked and measured for distortion.

The platinum resistance thermometer was installed on the bomb by means of a band on the outside of the bomb. This was assembled in the same manner as the bomb itself and was a .03 inch interference fit.

High-pressure seals

In performing these experiments one of the most difficult problems encountered was the design and fabrication of the electrical and bomb plug seals. The problem of containing helium gas under pressure at low temperature is well known to anyone who has worked in this field. Epoxy seals, which were sufficient for much of the range covered, had already been developed at this laboratory.[90]

It was desired, however, to develop an electrical seal which would be easier to work with than this type. The electrical seal which was finally used is shown in Figure 15 and is simply a logical next step from the ones previously developed. The earlier seals depended upon the bond between the epoxy and the tube to carry the shear load which prevented the seal from blowing out. The new seal has a large cross section in the middle so that the epoxy itself must fail for the seal to blow out.

In this seal, the wires pass through a small hole filled with an epoxy. (Eccobond 104) The tubing used in the seal was Harwood 3M and 12H. Standard Harwood cone and sleeve fittings which were good to pressures greater than 14 kilobars were used in all cases except where the 3M tubing mated to the 12H. One non-standard part, the gland nut, had to be made for this connection. It was made from type 304 stainless steel and had the dimensions shown in Figure 15. The 12H tubing was drilled, tapped and a 60° conical seat was made on each end. The 3M tubing was threaded and coned in the standard manner. In order to insure that the epoxy bonded to the tubing, the walls were etched with acid and cleaned with water and acetone. The wires used were number 36 quadruple formvar insulated copper. They were cleaned with acetone and placed inside the tube. Epoxy was mixed and forced into the tubes with the small stainless steel tube and screw

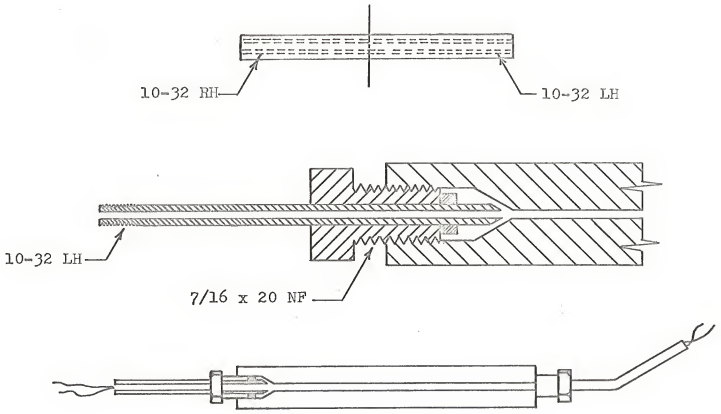

Figure 15. Electrical seal.

shown in Figure 15. The wires were moved slowly back and forth several times, the excess epoxy was removed and the seals were baked according to manufacturer's specifications. The seals were tested on a liquid pressure system before being used in the gas facility. All of them were tested to about 140,000 psi and none blew out. Two of them were taken to 200,000 psi and while no leaks developed the wires inside were broken by the epoxy shifting in the tube. The addition of 5-10 per cent alumina powder to the epoxy has been reported[91] to significantly increase its strength. This was tried but the one seal made in this way leaked at a low pressure. This may have been due to incomplete filling of the tube during fabrication. More work should be done on this since it seems that if the epoxy could be strengthened this should make a simple, inexpensive seal for gas systems up to 200,000 psi.

The plug seal offered even more difficulty than the electrical seals. Many variations were tried and discarded. The one finally used is shown in Figure 16 and is good to at least 100,000 psi. It will probably go higher but leakage in the intensifier seals have restricted the experiments to this pressure. It will be noted that it is a Bridgman unsupported area seal.[92] Some workers have reported that this seal will not work at low temperatures due to the fact that the indium metal contracts more than the beryllium copper upon cooling. It was found, however, that if the bomb was cooled while under pressure no leaks

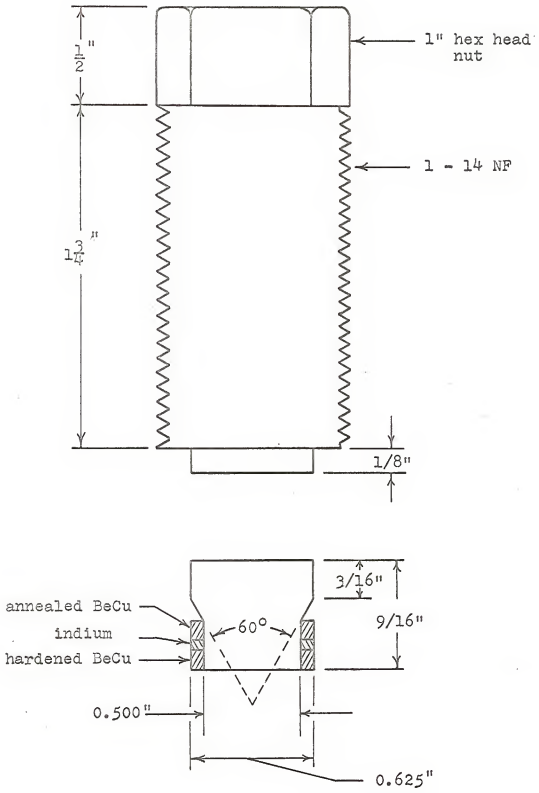

Figure 16. Bomb plug and seals.

would occur. This seal has the advantage that it seals with very low torque, is simple to machine, and is reusable many times. It consists of a lower support ring made of hardened beryllium copper, a ring of indium, and an upper extrusion ring of fully annealed beryllium copper. The plug is made of hardened beryllium copper.

Temperature Production and Measurement

The basic cryostat system, which was used in all of the experiments, is shown in Figure 17. Some modifications, to be described later, were necessary for running the lowest temperature transition. The basic system consisted of an outer nitrogen dewar, an inner nitrogen or helium dewar, and an evacuated can which contained the bomb. Aluminum foil, which has a low emissivity, was used to wrap the bomb and line the inner walls of the can. The inlet pressure line was stainless steel which has a low thermal conductivity at low temperatures. A non-inductively would heater coil was connected to the top of the bomb with woods metal. Three copper-constantan thermocouples were installed to measure the temperature of the bomb. The upper and lower ones used a copper lug on the wall of the can as a reference temperature while the middle one was brought out of the cryostat to a liquid

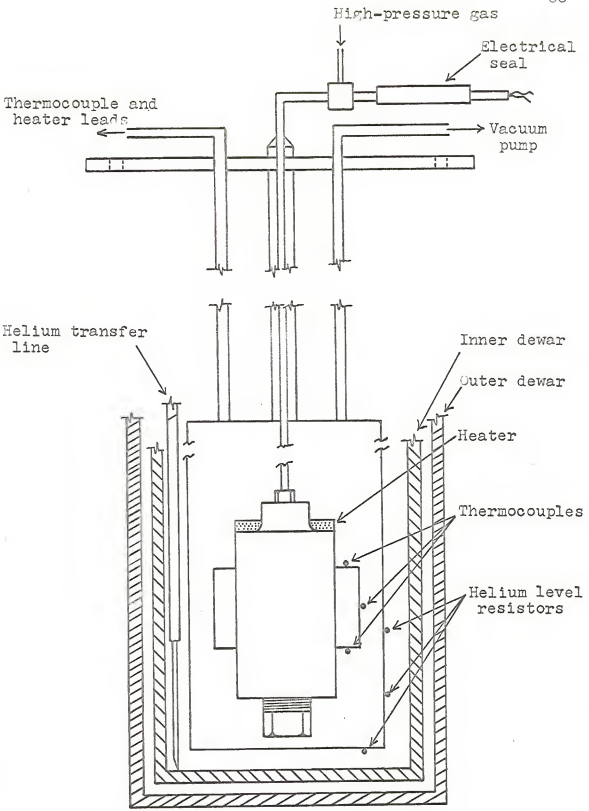

Figure 17. Cryostat.

nitrogen bath for reference. Periodically a platinum resistance thermometer was installed in the bomb and the thermocouples were checked. Temperature accuracy was judged to be $\pm.25^{\circ}K$ and reproductibility was better than $\pm.10^{\circ}K$.

In the experiments involving the Néel transition the inner dewar was filled with liquid nitrogen and exchange gas was allowed into the can containing the bomb. When the bomb had cooled to approximately the desired temperature the can was evacuated and thereafter maintained at a pressure of not more than .2 microns. With the bomb thus isolated the required temperature could be maintained with the heater.

In the experiment involving the Curie transition of dysprosium it was necessary to cool the sample down to about $60^{\circ}K$. This was done by pumping on the nitrogen bath with a large Kinney pump (Model No. KC-46). The temperature was then controlled by use of the heater.

The ferromagnetic transition in erbium, which occurs at about $20^{\circ}K$, made it necessary to use liquid helium and also required some modifications in the equipment. Two copper straps (dimensions 3 x .375 x .025 inches) were soldered to the bottom of the bomb and to the bottom of the can. In addition to this, a heater coil was wrapped around the inlet pressure line. With these two modifications it was possible to maintain a temperature gradient

across the bomb sufficient to insure that the helium froze from the bottom to the top.

Procedure

Procedure for experiments above 60°K.

The following procedure is applicable for experiments above 77°K. A modification of the procedure given at the end of this section allows for operation down to 60°K.

1. Place the sample in the coil and solder the coil leads onto the electrical leads in the bomb.
2. Clean the seals and install the plug in the bomb.
3. Wrap the bomb with aluminum foil and place the styrofoam spacer around the bomb.
4. Woods metal the can into place around the bomb. Check the system for leaks in the joints.
5. Lower the can into the inner dewar and bolt the flange into place.
6. Carry the dewar system into the pressure room and connect the pressure lines and all of the electrical leads.
7. Pressurize the system to a few hundred psi.
8. Fill the inner dewar and the thermocouple reference dewar with nitrogen.
9. After the bomb has been cooled to the desired temperature range evacuate the can containing the bomb and turn on the heater to control the temperature.

10. Take data points about every 0.1°K in the temperature region near the transition.
11. Top off the thermocouple reference dewar and fill the cold trap dewar with liquid nitrogen.
12. Connect the nitrogen dewar for remote transfer.
13. Close the blow down valve and plug in power cord.
14. To prepare for first pressure application open the charging solenoid valve to charge the pressure system from the 2,000 psi helium storage cylinder. Make sure that both the intensifier and the separator are cycled to the bottom of their stroke.
15. Close the charging solenoid valve and open the blow-down solenoid valve.
16. Pressurize the system with the separator for the first pressure point.
17. Slowly release the oil pressure in the separator.
18. Control the temperature with the heater and take readings at this pressure.
19. Activate the pump to the first separator.
20. Go to the desired pressure and take data.
21. After a run is complete bleed the pressure down very slowly. If the pressure is released rapidly the intensifier seals may be seriously damaged.

The procedure for work between 60°K and 77°K is the same as that outlined above except that the outer dewar is filled with liquid nitrogen and a vacuum pump is connected to the inner dewar.

Procedure for experiment below 60°K.

For work below 60°K it is necessary to use liquid helium and the procedure must be altered.

The first three steps are the same as listed before.

4. Fasten the copper thermal shorts to the bomb plug with woods metal.
5. Woods metal the alternate can, except for bottom onto the flange around the bomb.
6. Connect the copper straps to the bottom of the can and seal this onto the can walls. Check for leaks.
7. Insert the helium transfer line through fitting provided in the flange.
8. Lower the can into the dewar and fasten the top with bolts.
9. Carry the dewars into the pressure room and connect all lines and electrical connections.
10. Pressurize the system to a few hundred psi.
11. Fill the inner, outer and thermocouple reference dewars. Let the system cool to about 77°K.
12. Transfer the liquid nitrogen out of the inner dewar and connect the liquid helium dewar for remote transfer.
13. Start the transfer. A flow meter and a bubbler can be used in the recovery line from the helium cryostat to determine the rate at which the transfer is progressing.
14. Set the micrometer needle valve on the bottom of the control panel so that the pressure gauge on the line

supplying helium for the transfer indicates 3 psi or less. The micrometer valve gives fairly fine control, and the rate of cool down can be controlled by adjusting it.

15. After the system has cooled appreciably below 77°K evacuate the can surrounding the bomb.
16. As the temperature of the bomb reaches the freezing temperature of the helium inside it turn on the heater on the inlet pressure line and on the top of the bomb. Transfer slowly and maintain the top of the bomb several degrees above the bottom. Continue this until well below the freezing temperature to insure that the helium freezes from the bottom to the top of the bomb.
17. After the lowest temperature desired is obtained it can be maintained or allowed to increase slightly by varying the helium transfer rate.
18. Data can be taken while cooling or warming.
19. If it is desired to increase the pressure it is necessary to warm to a temperature greater than the freezing temperature of helium at the desired pressure.
20. Pressurize by following 13-17 of the previous section.
21. Steps 13-18 of this section are then repeated.

CHAPTER IV

RESULTS AND CONCLUSIONS

Introduction

The data taken in this study fall quite naturally into two categories. The higher temperature transitions (Néel transitions) and the lower temperature transitions (Curie transitions). The Néel transitions are, as discussed in Chapter II, mainly caused by the indirect exchange mechanism and are second order phase transitions. The Curie transitions are due to the temperature variations of the anisotropy energy and are first order phase transitions. The first section of this chapter presents the data obtained on the Néel transitions followed by a comparison with the available theories. The second section does the same with the Curie transition data. The final section is a discussion of the conclusions drawn from the results.

Néel Transitions

Results

The Néel transition occurs at about 179°K for dysprosium and was the first one studied. This transition

was found to be sharp and reversible. Figure 18 shows a run for dysprosium at atmospheric pressure over a temperature range great enough to show both transitions. In determining the Neel transition temperature it was necessary to traverse only about one degree in temperature. The height of the peak was depressed and the location shifted by the application of pressure. Figure 19 shows a typical run at atmospheric pressure and at 25,000 psi. The peak was located in the following way. In the region near the maximum, pairs of temperatures corresponding to points of the same inductance on either side of the maximum were read from the graph. The locus of the mean of these pairs was extrapolated to intersect the experimental curve. This procedure is indicated in Figure 19. It was necessary to rerun the atmospheric pressure peak each time the apparatus was reassembled as the location of the transition varied somewhat from one assembly to the next. This was probably due to small variations in the way the thermal gradients arranged themselves each time. The shifts were obtained for each pressure at least twice and in some cases numerous times. The value of the shift was found to be reproducible to within .04°K at a given pressure. The pressure shift for dysprosium is presented in Figure 20. Each of the determinations fell within the datum point shown. The average shift was found to be $dT_N/dP = -0.44 \pm 0.01$ °K/kilobar.

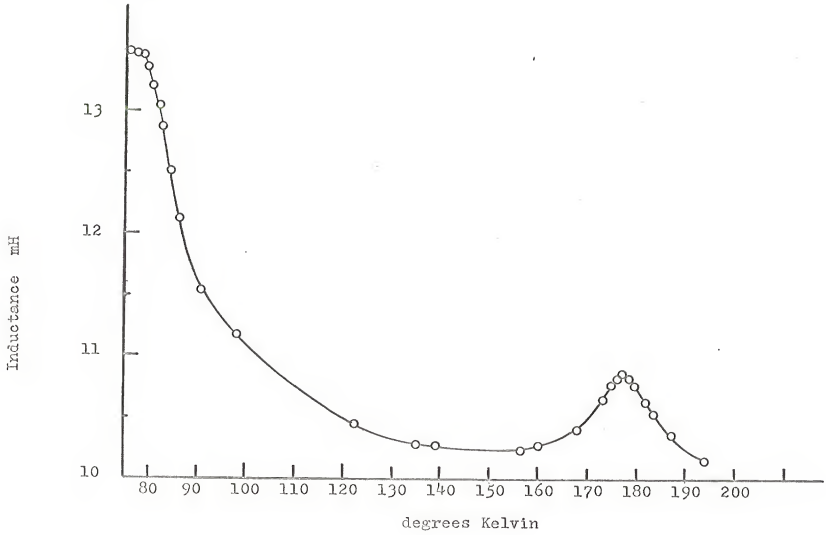

Figure 18. Inductance versus temperature for dysprosium.

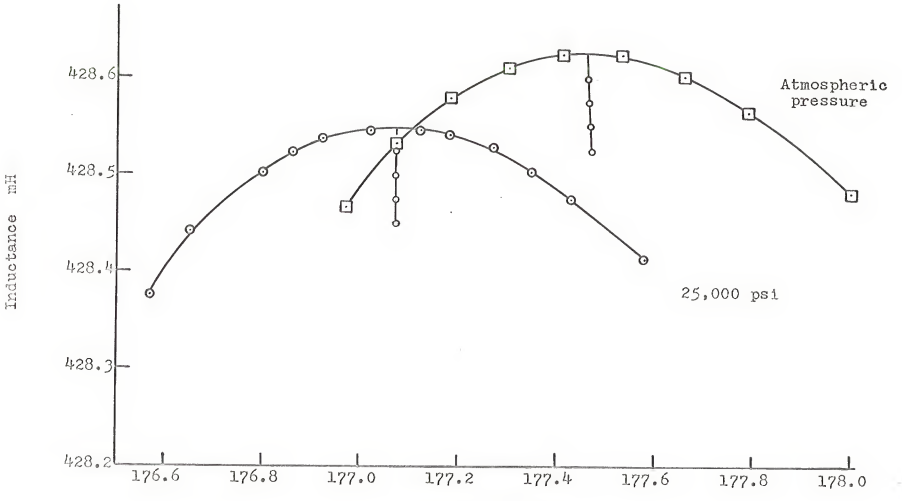

Figure 19. Néel transition for dysprosium.

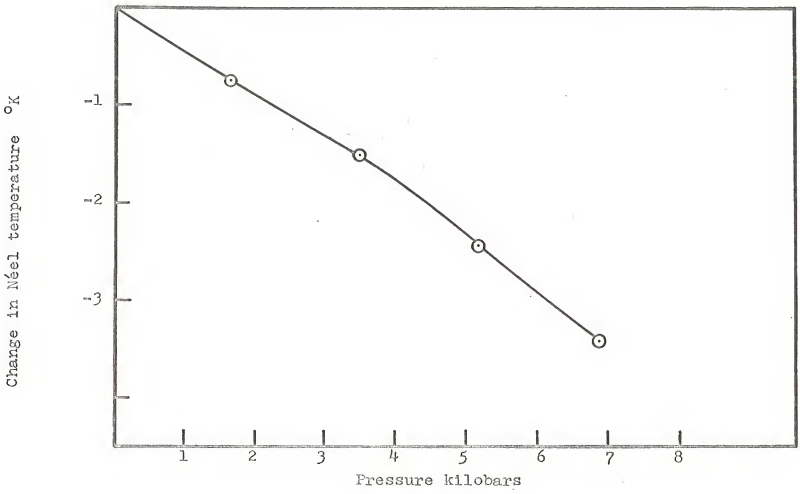

Figure 20. Pressure shift of Néel transition for dysprosium.

The data for the Néel transition for erbium, which occurs at about 85°K, were also sharp and reversible. The shift for erbium was found to be $dT_N/dP = -0.26 \pm 0.01$ °K/kilobar and is presented in Figure 21.

Comparison of results with theory

It is possible, as shown in Chapter II, to calculate the value of dT_N/dP by using the theory of second order phase transitions.

By using the expression,

$$\frac{dT_N}{dP} = \frac{3T_N}{\rho} \frac{\Delta\alpha}{\Delta C_p}$$

where $\Delta\alpha$[93] is the height of the thermal expansion anomaly, ΔC_p[94] is the height of the specific heat anomaly, and ρ [95] is the density, it was possible to calculate $dT_N/dP = -0.45$ °K/kilobar for dysprosium. The excellent agreement between the calculated value and the experimental value is perhaps better than should be expected since the data for $\Delta\alpha$ are not that accurate. The $\Delta\alpha$ is unfortunately unknown for erbium so it is not possible to calculate the shift in this case.

The interaction curve of Robinson et al. as shown in Figure 22 would seem to predict a positive value for the shift in dysprosium and erbium. As pointed out in Chapter II there is some uncertainty as to just what value for the transition temperature should be used in this theory. In any case our data do not agree with this positive value.

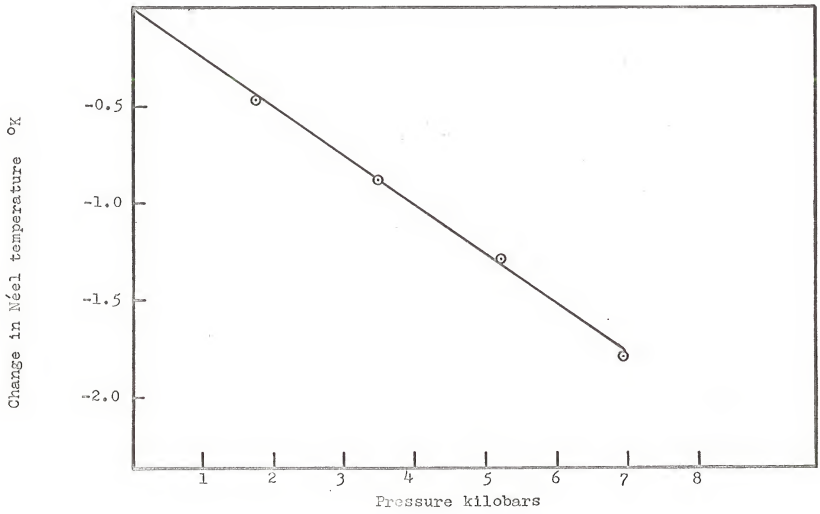

Figure 21. Pressure shift of Néel transition for erbium.

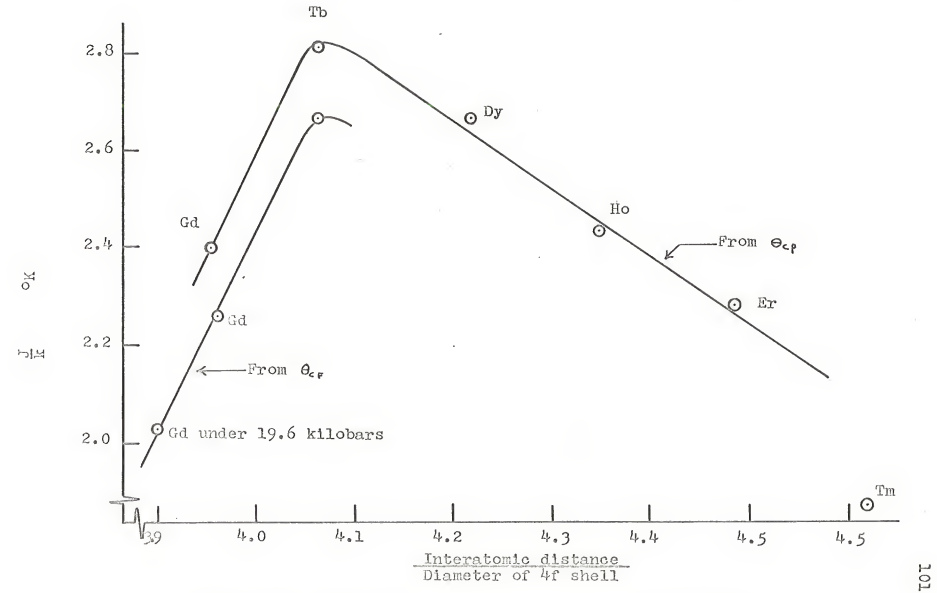

Figure 22. Robinson's interaction curve for rare earths.

McWhan[40] has suggested that it would be desirable to construct an interaction curve for the highest transition from which the dependence of the ordering temperature upon J, L and S has been eliminated. This can be done by dividing T by $(g-1)^2 J(J+1)$, the De Gennes function.[62] Such an interaction curve is presented in Figure 23. Without detailed knowledge of the compressibility of dysprosium and erbium in this temperature range it is not possible to accurately calculate what the shifts would be according to this theory. It can be seen, however, that the proper sign is predicted. By using Bridgman's room temperature compressibilities, $\beta = 2.74$ and 2.63×10^{-6} cm^2/kg for dysprosium and erbium respectively, it was possible to calculate $dT_N/dP = -0.64$ °K/kilobar for dysprosium and $dT_N/dP = -0.29$ °K/kilobar for erbium. In view of the uncertainties involved in using these compressibility data at low temperatures the agreement seems to be quite good. The important point is that not only is the proper sign predicted but also the shift for erbium is predicted to be smaller than that for dysprosium.

McWhan has calculated $\frac{d \ln T}{d \ln V}$ for all of the experiments that have previously been done on the rare earths. He has found that the points fall on two distinct curves with a break between europium and gadolinium. This break is probably associated with the fact that the lighter rare earths have a modified hexagonal crystal structure. The results of McWhans calculations with the data from this work on erbium and dysprosium added are presented in Figure 24.

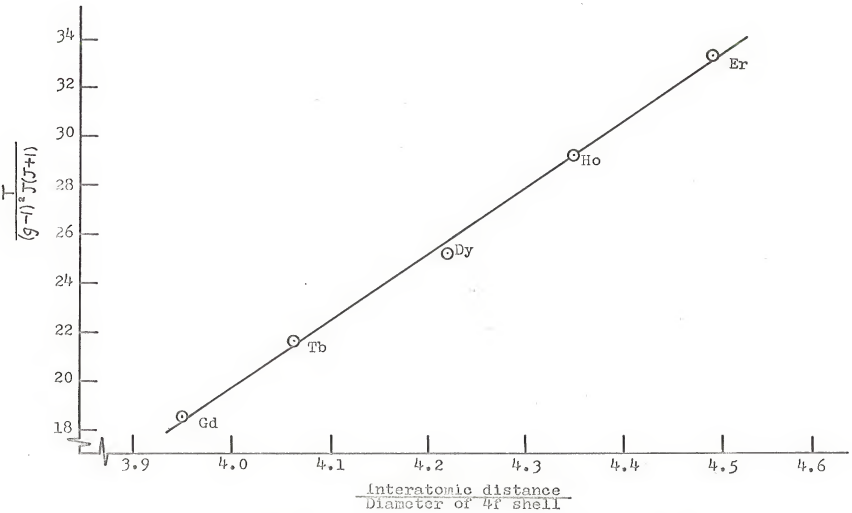

Figure 23. Interaction curve for rare earths.

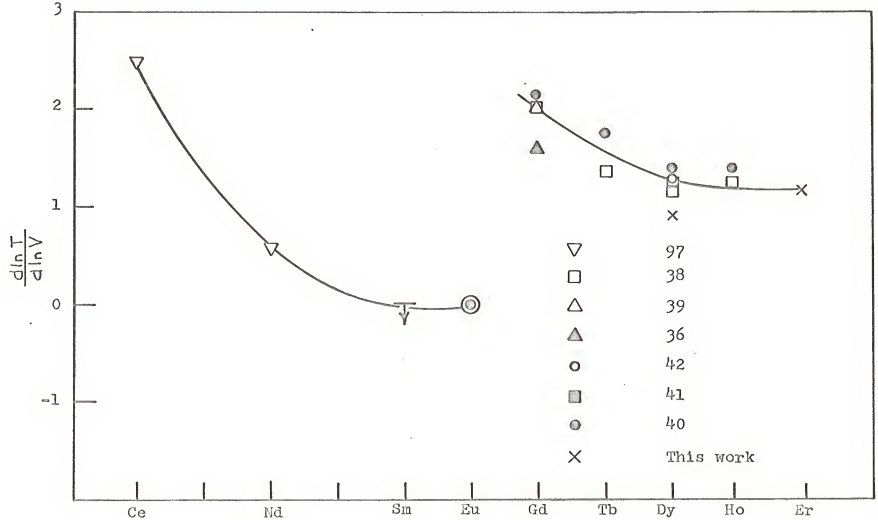

Figure 24. $\frac{d\ln T}{d\ln V}$ for rare earths.

All of the points except gadolinium are calculated for Néel temperatures.

Curie Transitions

Results

The ferromagnetic transition for dysprosium was much more difficult to work with than the Néel transition. The data taken while cooling were found to differ by about 10°K from data taken while warming. Even more disturbing was the fact that if the sample was taken to a temperature near the transition and held there the inductance values would continue to change for a long time. A test was run at 77°K and it was found that the inductance was still changing slowly at the end of three and a half hours. This result made it undesirable to use the method of extrapolating the straight line portion of the curve to where it intercepted the temperature axis for determining the transition temperature. The extrapolation method has been used quite successfully to determine pressure shifts of transition with some materials.

It was found that if dysprosium was cooled to about 60°K, far below its transition temperature, and then the data were taken while warming the sample the results were reproducible and the inflection point of the inductance versus temperature curve occurred at 85°K. This value is in

good agreement with other magnetic measurements.[19] Several heating rates were tried and were found not to change the location of the transition. All of the data used in determining dT_c/dP were taken at a warming rate of about 6 degrees per hour. The experimental curves are presented in Figure 25 and dT_c/dP is given in Figure 26. Over the pressure range studied the shift was found to be $dT_c/dP = -1.2$ ^{o}K/kilobar.

The data on erbium for its low temperature transition is presented in Figures 27 and 28. As can be seen the shape of the curve for cooling data is completely different from that of the warming data. The reasons for this difference is not understood at the present time. A similar situation was found by Adams and Green[27] when they studied meteoric iron. The upper peak on the warming curve corresponds to an anomaly found at 52^{o}K by both neutron diffraction and electrical resistivity experiments.[19] From the neutron diffraction work it has been concluded that between 80^{o}K and 52^{o}K only the c component of the magnetic moment is modulated sinusoidally along the c-axis. Sinusoidal modulation of the perpendicular component begins at temperatures lower than 52^{o}K.

The lower peak in the warming curve occurs at 20^{o}K and would therefore seem to correspond to the ferromagnetic transition. The fact that the middle peak on the warming curve has not been reported in high field magnetic measurements is perhaps not too surprising since these experiments

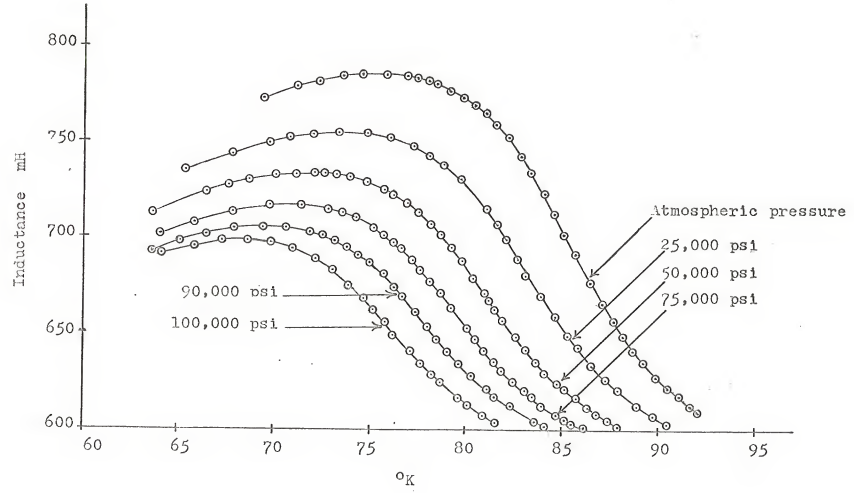

Figure 25. Dysprosium data.

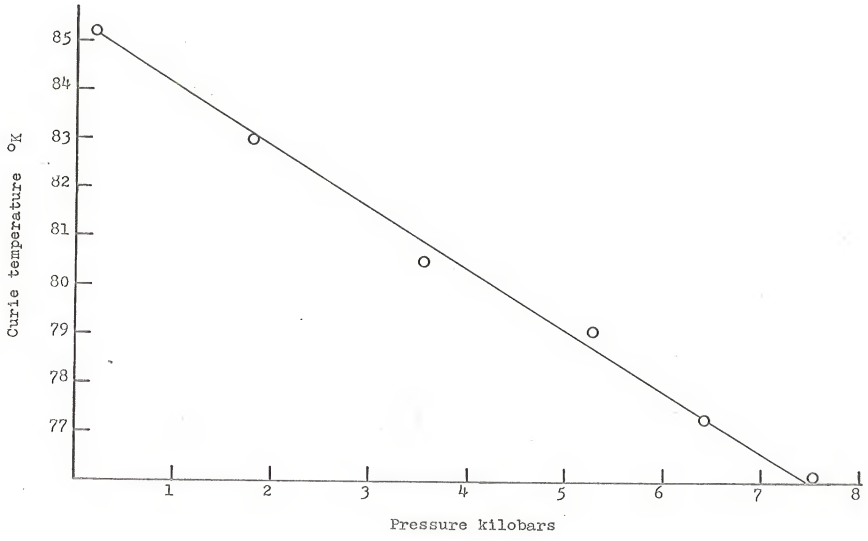

Figure 26. Pressure shift of Curie transition for dysprosium.

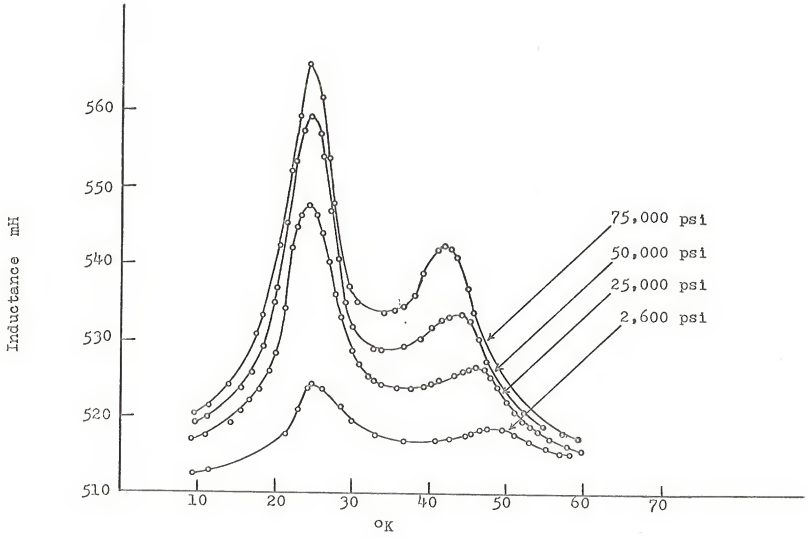

Figure 27. Erbium data taken while cooling.

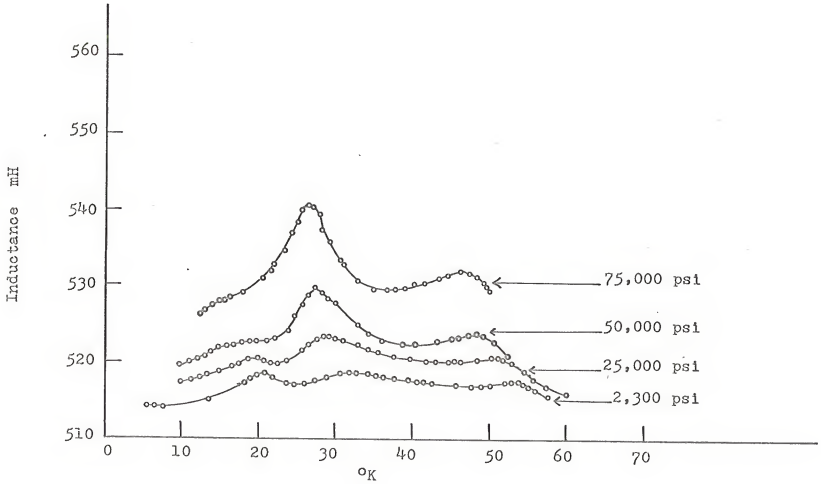

Figure 28. Erbium data taken while warming.

do not detect the 52°K transition either. It is curious that it has not been seen by the neutron diffraction studies since it is about the same magnitude as the other two peaks. The upper cooling peak probably corresponds to the 52 degree transition with a shift due to rate effects. The tremendous peak found at 24.2°K in the cooling curve is quite surprising. The pressure shifts of these peaks are presented in Figures 29, 30 and 31. The large lower peak in the cooling curve showed no shift with pressure while all of the others did. A blank run was made in order to insure that none of the anomalies that were observed were due to the apparatus.

Comparison of results with theory

The theory, as developed by Liu, for the shift in the paramagnetic Curie temperature for rare earths can only be examined qualitatively here. Unfortunately the data were not taken in a way that allows an accurate determination of this temperature and even if it had been, the compressibilities are not known in this region of temperature. Swenson has calculated $\frac{d \ln T}{d \ln V}$ by using the temperature at which the material actually goes ferromagnetic instead of the paramagnetic Curie temperature. The results of his calculations with the one for dysprosium and erbium from this work added are given in Figure 32. The results do not show the constant value predicted by Liu's theory but this could be due to not having data on the paramagnetic Curie temperature.

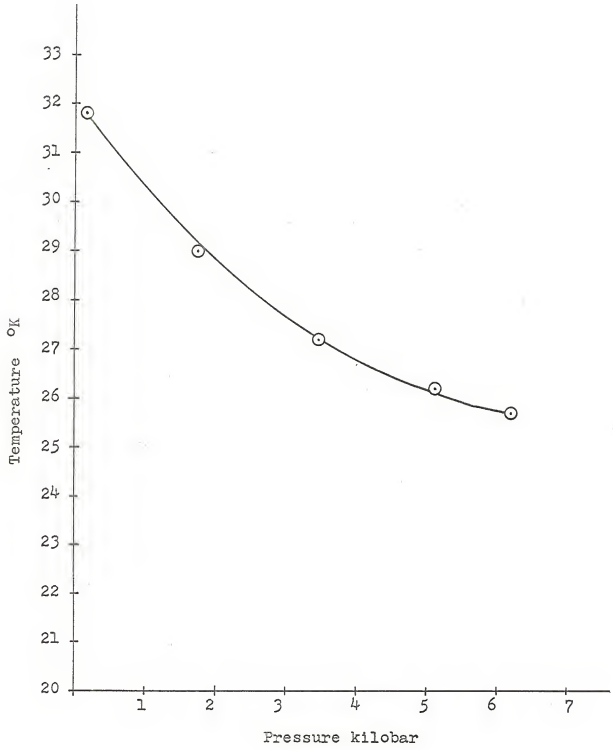

Figure 29. Pressure shift for middle peak on warming data for erbium.

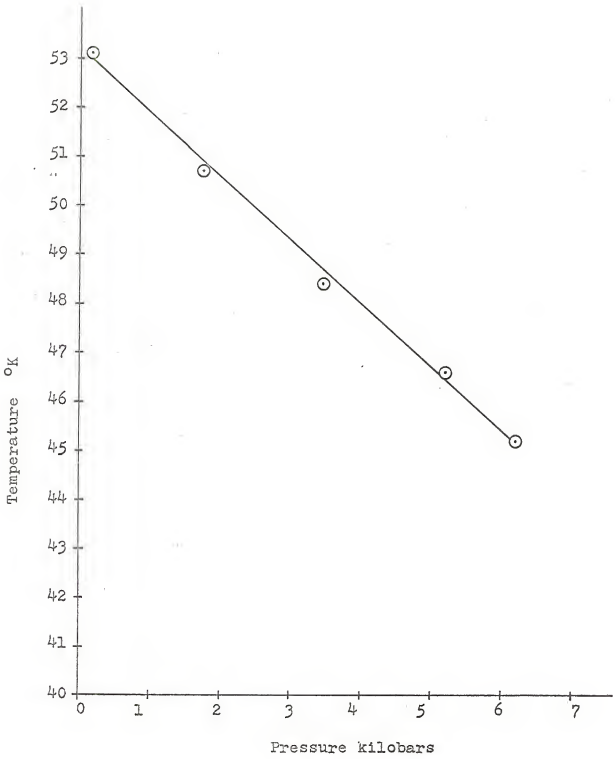

Figure 30. Pressure shift for upper peak on warming data for erbium.

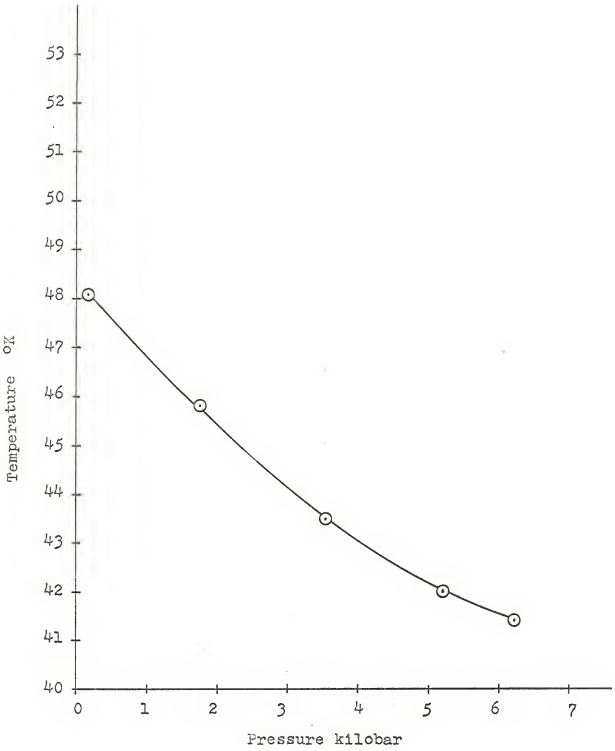

Figure 31. Pressure shift for upper peak on the cooling data for erbium.

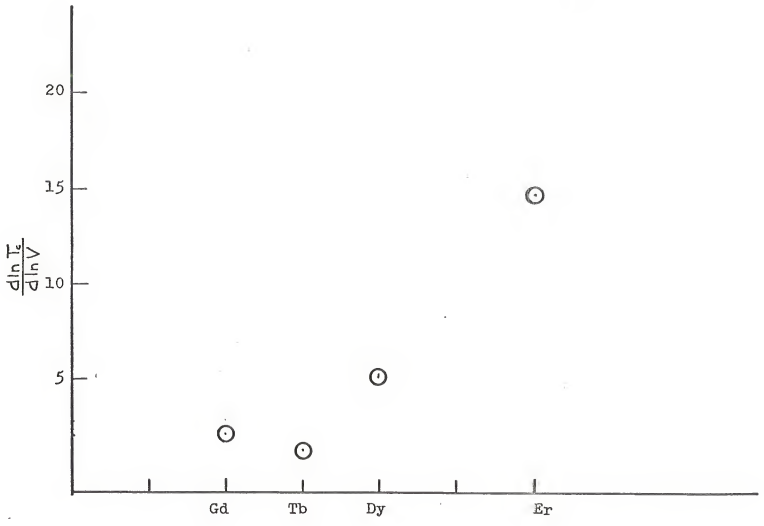

Figure 32. $\frac{d \ln T_c}{d \ln V}$ for heavy rare earths.

Conclusions

The agreement between the experimental and thermodynamically calculated shift for the Néel transition in dysprosium is quite encouraging. It would be desirable to have a more accurate determination of the height of the thermal expansion anomaly for dysprosium in order to determine if this result is valid. Of course the same information is needed for erbium.

The qualitative predictions based upon the interaction curve, Figure 22, formulated by Robinson et al.[43] are found to be violated by the data for both dysprosium and erbium.

The interaction curve given by Figure 23 which was constructed following a suggestion by McWhan[40] predicts shifts of the magnetic transition temperatures that are in fair agreement with the experimental ones. This curve is based, however, on a phenomenological approach and is therefore not as pleasing as one based upon first principles. In it no account is taken of the strong anisotropic forces which exist in the antiferromagnetic and ferromagnetic states of the rare earths.

There has been, as yet, no explanation given for the grouping of the values of $\frac{d\ln T}{d\ln V}$ as given in Figure 24. It is hoped that in the near future some theoretical basis can be given for this result.

While Liu's theory for the pressure dependence of the magnetic transitions in the heavy rare earths is open to objection on several points, it is based upon first principles and is a start in the explanation of these phenomena. The present theories indicate that anisotropy has a powerful influence on the magnetic properties of the rare earths. This would indicate that some further modifications must be made to make Liu's theory more realistic. He has based his theory on the premise that the indirect exchange mechanism causes the transitions, and that the ground state of the system due to the indirect exchange is ferromagnetic. This is not in keeping with the mainstream of the theoretical development which indicates the ferromagnetic transitions are probably caused by the anisotropic influences. Of course, as more information becomes available on the conduction electron properties there will probably be a need to modify the form chosen to represent their wave functions. This may quite likely bring in more terms with pressure dependence, for instance $\sum_i F(2k_F R_i)$ in equation 2.51 may have to be considered. In fairness it must be said that the above is speculative since no accurately determined data are available to test Liu's prediction. Here it is perhaps appropriate to quote from a paper by Monfort and Swenson[96] in regard to these predictions. "There is need for precise data in order to verify this prediction, and except for gadolinium, the existing data for the rare earths merely serve to give an

order of magnitude for what is a very small effect." In addition to precise data on dT/dP it will be necessary to have compressibility data in the region of the transition.

If single crystals could be obtained it would be very useful to do pressure studies on them since according to Landau's thermodynamic theory[52] $\frac{\theta_{p\perp} - \theta_{p\parallel}}{\theta_{p\parallel}}$ gives the ratio of the magnetic anisotropy energy to the magnetic exchange interaction energy. Where θ_p is the paramagnetic Curie temperature and $\parallel$ refers to measurements made parallel to the c-axis and $\perp$ perpendicular to it. This would seem to give a powerful tool to check the qualitative predictions of present theories.

The results for dT_N/dP for dysprosium are in general agreement with those reported previously and shown in Table 1. The dT_N/dP for erbium is new but seems to be quite reasonable according to phenomenological theories. The results on dT_c/dP for dysprosium are in agreement with some unpublished data by Swenson but in marked disagreement with those of Robinson et al.,[43] who find a positive shift for low pressures and a negative shift at high pressure. The appearance of the new peaks in the erbium data at low temperature are not understood and it is recommended that further study be given to this point.

In view of the fact that anisotropy is important and internal strains in the material could set up disturbances in the internal potentials of the material it would

seem very desirable to rerun the low temperature transition in erbium with a fully annealed sample to see if the previously unreported peaks are still present.

The accomplishments of this work are listed below.

1. A high-pressure gas system capable of generating hydrostatic pressures at low temperatures was designed, constructed and made operational. It should be a basic tool in many experiments in future years.

2. A new method for studying pressure shifts of magnetic transitions was developed. The necessary equipment for doing these studies was constructed and brought to the point where they work dependably.

3. Accurate measurements were made for dT_N/dP for dysprosium and erbium and dT_c/dP for dysprosium. Preliminary results were obtained for dT_c/dP for erbium.

4. The way was opened and experiments have been suggested which should be very fruitful in further checking theories of magnetic transitions.

5. Publications related to this dissertation: A note describing fabrication of a simple, inexpensive high pressure gas electrical seal is being prepared; also a paper is in progress describing the experimental results of this dissertation.

REFERENCES

1. G. Sarton, Introduction to the History of Science (Baltimore, 1927), Vol. I.

2. Lucretius Carus, De rerum natura (circa 70 B.C.).

3. Peregrinus de Maricourt, "Epistola Petri Peregrini de Foucancourt Militem de Magnete" (1269).

4. C. A. Coulomb, Collection des Memoires Relatifs a la Physique 1 (1884).

5. S. D. Poisson, Mem. de l'Acad. 5, 247.

6. W. Weber, Abhandlungen der Kg. Sachs Gesellschaft der Wissens, i.p. 572 (1852).

7. P. Curie, Ann. Chim. Phys. (7) 5, 289 (1895).

8. P. Langevin, Ann. Chim. Phys. (8) 5, 70 (1905).

9. L. Brillouin, J. Phys. Radium 8, 74 (1927).

10. P. Weiss, J. de Phys. (4) 6, 661 (1907).

11. P. A. M. Dirac, Proc. Roy. Soc. 117A, 610 (1928).

12. W. Heisenberg, Z. Physik. 38, 411 (1926).

13. E. Ising, Z. Physik 31, 253 (1925).

14. F. Bloch, Z. Physik 61, 206 (1930).

15. J. C. Slater, Phys. Rev. 35, 509 (1930).

16. L. Neel, Ann. Phys. (Paris) 17, 64 (1932).

17. K. A. Gschneidner, Jr., "Crystallography of the Rare Earth Metals," The Rare Earths, ed. F. H. Spedding and A. H. Doane (John Wiley & Sons, Inc., New York, 1961), Chapt. 14, p. 192.

18. K. A. Gschneidner, Jr., Rare Earth Alloys (D. van Nostrand Company, Inc., New York, 1961), Chapt. 1, p. 6.

19. R. J. Elliott, "Theory of Magnetism in the Rare Earth Metals," Magnetism, Vol. IIA, ed. G. T. Rado and H. Suhl (Academic Press, 1965), p. 389.

20. M. K. Wilkinson et al., J. Appl. Phys. 31, 49S (1961).

21. W. Koehler et al., Rare Earth Research (Macmillan, New York, 1961), p. 149.

22. W. Koehler, J. Appl. Phys. 31, 20S (1961).

23. W. Koehler et al., J. Phys. Soc. Japan 17, 32S (1962).

24. W. Koehler et al., J. Appl. Phys. 31, 48S (1961).

25. W. Koehler et al., Phys. Rev. 126, 1672 (1962).

26. G. Will et al., J. Appl. Phys. 35, 1045 (1964).

27. L. H. Adams and J. W. Green, Phil. Mag. 12, 361 (1931).

28. J. S. Kouvel, "Magnetic Properties of Solids Under Pressure," Solids Under Pressure, ed. W. Paul and D. M. Warschauer (McGraw-Hill, New York, 1963), pp. 277-295.

29. C. Yeh, Proc. Am. Acad. Arts Sci. 60, 503 (1925).

30. R. L. Steinberger, J. Appl. Phys. 4, 153 (1933).

31. A. Michels et al., Physica 4, 1007 (1937).

32. A. Michels and J. Strijland, Physica 8, 53 (1941).

33. F. Ebert and A. Kussman, Physik. Z. 39, 598 (1938).

34. A. Michels and S. R. de Groot, Physica 16, 249 (1950).

35. M. Kornetzki, Z. Physik 98, 289 (1935).

36. L. Patrick, Phys. Rev. 93, 384 (1954).

37. G. A. Samara and A. A. Giardini, Rev. Sci. Instr. 36, 108 (1965).

38. D. Bloch and R. Pauthenet, Compt. Rend. 254, 1222 (1962).

39. L. B. Robinson et al., Phys. Rev. 134, A187 (1964).

40. D. B. McWhan and A. L. Stevens, "The Effect of Pressure on the Magnetic Properties and Crystal Structure of Gd, Tb, Dy and Ho." (Unpublished paper presented at A.P.S. meeting, New York, 1965)

41. P. Landry and R. Stevenson, Can. J. Phys. 41, 1273 (1963).

42. P. C. Sovers and G. Jura, Science 145, 575 (1964).

43. L. B. Robinson et al., Phys. Rev. 141, 548 (1966).

44. K. P. Belov et al., Soviet Phys. JETP 45, 26 (1963).

45. A. J. Dekker, Solid State Physics (Prentice-Hall, Inc., Englewood Cliffs, N. J., 1957), Chapt. 19, pp. 464-488.

46. F. Seitz, The Modern Theory of Solids (McGraw-Hill Book Company, Inc., New York, 1940), Chapt. 16, pp. 576-627.

47. C. Kittel, Introduction to Solid State Physics (John Wiley & Sons, Inc., New York, 1956), 2nd ed., Chapt. 15, pp. 402-450.

48. J. B. Goodenough, Magnetism and the Chemical Bond (Interscience Publishers, New York, 1963), Chapt. 2, pp. 75-156.

49. R. M. Bozorth, Ferromagnetism (D. van Nostrand Company, Inc., New York, 1951).

50. F. H. Spedding et al., "Some Physical Properties of the Rare Earth Metals," Progress in Low Temperature Physics, Vol. 2, ed. C. J. Gorter (Interscience Publishers Inc., New York, 1957), pp. 368-394.

51. D. C. Mattis, The Theory of Magnetism (Harper & Row, New York, 1965), Chapt. 2, pp. 31-55.

52. K. P. Belov et al., Soviet Phys.-Usp. 7, 179 (1964).

53. L. B. Robinson et al., "Magnetic Behavior of Rare Earth Metals at High Pressures," Physics of Solids at High Pressures, ed. C. T. Tomizuka and R. M. Emrick (Academic Press, New York, 1965), pp. 272-294.

54. R. J. Elliott, "Theory of Magnetism in the Rare Earth Metals," Magnetism, Vol. IIA, ed. G. T. Rado and H. Suhl (Academic Press, 1965), p. 389.

55. K. Yosida, "Magnetic Structures of Heavy Rare-Earth Metals," Progress in Low Temperature Physics, Vol. 4, ed. C. J. Gorter (Interscience Publishers, Inc., New York, 1964), pp. 265-295.

56. J. H. van Vleck, The Theory of Electric and Magnetic Susceptibilities (Oxford University Press, London, 1932), Chapt. 2, pp. 27-41.

57. S. Chikazumi, Physics of Magnetism (John Wiley & Sons, Inc., New York, 1964), Chapt. 20, pp. 440-458.

58. L. D. Landau, Z. Physik 64, 629 (1930).

59. L. Néel, Ann. Phys. (Paris) 5, 232 (1936).

60. F. Bitter, Phys. Rev. 54, 79 (1937).

61. J. H. van Vleck, J. Chem. Phys. 9, 85 (1941).

62. P. G. de Gennes, Compt. Rend. 247, 1836 (1958).

63. R. Brout and H. Suhl, Phys. Rev. Letters 2, 387 (1959).

64. G. S. Anderson and S. Legvold, Phys. Rev. Letters 1, 322 (1958).

65. T. A. Kaplan, Phys. Rev. 125, 329 (1961).

66. R. J. Elliott, Phys. Rev. 124, 346 (1961).

67. K. Yosida and H. Miwa, Progr. Theoret. Phys. (Kyoto) 26, 693 (1961).

68. R. J. Elliott, Phys. Rev. 124, 346 (1961).

69. K. W. H. Stevens, Proc. Phys. Soc. (London) A 65, 209 (1952).

70. A. J. Freeman and R. E. Watson, Phys. Rev. 127, 2058 (1962).

71. H. Miwa and K. Yosida, J. Phys. Soc. Japan 17, Suppl. B-I, 5 (1962).

72. U. Enz, Physica 26, 698 (1960).

73. T. A. Kaplan and D. H. Lyons, Phys. Rev. 129, 2072 (1963).

74. T. Kasuya, Progr. Theoret. Phys. (Kyoto) 16, 45 (1956).

75. K. Yosida, Phys. Rev. 106, 893 (1957).

76. S. H. Liu, Phys. Rev. 121, 451 (1961).

77. L. D. Landau and E. M. Lifshitz, Quantum Mechanics, trans. J. B. Sykes and J. S. Bell (Addison-Wesley Publishing Company, Inc., 1958), Chapt. 9, p. 211.

78. L. Pauling, Proc. Roy. Soc. (London) A 114, 181 (1927).

79. L. Néel, Compt. Rend. 206, 49 (1938).

80. S. H. Liu, Phys. Rev. 127, 1889 (1962).

81. M. A. Ruderman and C. Kittel, Phys. Rev. 96, 99 (1954).

82. M. W. Zemansky. Heat and Thermodynamics (McGraw-Hill Book Company, Inc., New York, 1957), Chapt. 15, pp. 317-338.

83. A. M. Thompson, IRE Trans. on Instrumentation 1, 245 (1958).

84. M. C. McGregor et al., IRE Trans. on Instrumentation 1, 253 (1958).

85. R. E. Travis and J. A. Zugel, "Ratio Transformers, Theory, Design and an Application," Precision Measurements Course (The Boeing Company, Aerospace Division, Seattle, Washington, 1962), Session 26.

86. D. L. Hillhouse and H. W. Kline, IRE Trans. on Instrumentation 9, 251 (1960).

87. J. S. Dugdale and F. E. Simon, Proc. Roy. Soc. (London) A 218, 291 (1953).

88. O. L. Anderson, Some Safety Problems Associated with High Pressure Equipment (Unpublished technical memorandum, Case 38143, Bell Telephone Laboratories, 1954).

89. S. Timoshenko, Strength of Materials (D. van Nostrand Company, Inc., New Jersey, 1956), part 2, p. 205.

90. W. S. Goree, B. McDowell and T. A. Scott, Rev. Sci. Instr. 36, 99 (1965).

91. L. A. Davis et al., Rev. Sci. Instr. 35, 368 (1964).

92. P. W. Bridgeman, The Physics of High Pressure (G. Bell & Sons, Ltd., London, 1958).

93. F. Barson et al., Phys. Rev. 105, 418 (1957).

94. M. Griffel et al., J. Chem. Phys. 25, 75 (1956).

95. F. H. Spedding et al., "Some Physical Properties of the Rare Earth Metals," Progress in Low Temperature Physics, Vol. 2, ed. C. J. Gorter (Interscience Publishers Inc., New York, 1957), pp. 370-371.

96. C. E. Monfort III and C. A. Swenson, J. Phys. Chem. Solids 26, 623 (1965).

BIOGRAPHICAL SKETCH

James E. Milton was born May 12, 1934, at Florala, Alabama. In June 1951, he was graduated from Columbia High School in Lake City, Florida. He attended the University of Florida intermittently from 1951 - 1954. From 1955 until 1958 he served in the United States Army. Following his discharge from the Army, he returned to the University of Florida. In June 1960, he received the degree of Bachelor of Aeronautical Engineering. From September 1960, until the present time he has pursued his work toward the degree of Doctor of Philosophy.

James E. Milton is married to the former Mary Eleanor Jernigan and is the father of two children.

This dissertation was prepared under the direction of the chairman of the candidate's supervisory committee and has been approved by all members of that committee. It was submitted to the Dean of the College of Arts and Sciences and to the Graduate Council, and was approved as partial fulfillment of the requirements for the degree of Doctor of Philosophy.

April, 1966

E. Rudolph Jones
Dean, College of Arts and Sciences

Dean, Graduate School

Supervisory Committee:

J. A. Scott
Chairman

E. D. Adams

W. S. Bray

E. H. Hadlock